Duke-CGTP-04-09
TIFR-TH-04-26
hep-th/0412337

On tachyons, gauged linear sigma models, and flip transitions

David R. Morrison[a] and K. Narayan[a,b]

[a] *Center for Geometry and Theoretical Physics,*
Duke University,
Durham, NC 27708, USA.

[b] *Tata Institute of Fundamental Research,*
Homi Bhabha Road,
Colaba, Mumbai - 400005, India.

Email: drm, narayan@cgtp.duke.edu, narayan@theory.tifr.res.in

Abstract

We study systems of multiple localized closed string tachyons and the phenomena associated with their condensation, in $\mathbb{C}^3/\mathbb{Z}_N$ nonsupersymmetric noncompact orbifold singularities using gauged linear sigma model constructions, following hep-th/0406039. Our study reveals close connections between the combinatorics of nonsupersymmetric flip transitions (between topologically distinct resolutions of the original singularity), the physics of tachyons of different degrees of relevance and the singularity structure of the corresponding residual endpoint geometries. This in turn can be used to study the stability of the phases of gauged linear sigma models and gain qualitative insight into the closed string tachyon potential.

Contents

Both from the point of view of gaining a deeper understanding of the vacuum structure of string theory as well as other angles such as understanding the role of time in string theory, the analyses of tachyon dynamics that have emerged over the last few years following Sen [1] have been particularly insightful (see, *e.g.*, [1, 2, 3] for general reviews of tachyon condensation). Ideally one would like to gain insight into the dynamics of tachyonic instabilities in string theory by studying their evolution in time: this is however quite hard in general. Thus one needs to resort to other techniques that are more amenable to precise calculation. In particular, considerable qualitative insight into the physics is gained by replacing the on-shell question of time evolution of a stringy system with the off-shell question of studying the "space of string theories" via off-shell formulations, such as string field theory (see, *e.g.*, [1, 4]) or string worldsheet renormalization group flow approximated by an appropriate gauged linear sigma model (GLSM) (see, *e.g.*, [5, 6]) and their mirror descriptions (see, *e.g.*, [6]).

These issues are complicated still further for closed string tachyons where one could *a priori* suspect delocalized tachyonic instabilities to lead to the decay of spacetime geometry itself, by analogy with open string tachyons which lead to D-brane decay. In this regard, an important set of developments was the realization of the endpoint of condensation of tachyons *localized* to nonsupersymmetric noncompact $\mathbb{C}/\mathbb{Z}_N$ and $\mathbb{C}^2/\mathbb{Z}_N$ orbifold singularities [7, 8, 9]. Since the tachyon is localized to the singularity, its condensation can be expected to initially

affect only the immediate vicinity of the singularity: and in fact, rather than leading to any uncontrolled behaviour, the process of tachyon condensation smooths out and resolves the singularity. Furthermore the physical question of tachyon condensation in these orbifold theories is closely intertwined with the algebro-geometric structure of the singularities [9] so that the known mathematics of Kähler deformations can be used to study the physics of condensation of tachyons when the condensation preserves worldsheet supersymmetry. The corresponding question for nonsupersymmetric $\mathbb{C}^3/\mathbb{Z}_N$ singularities [10] is potentially somewhat more complicated due to the existence of geometric terminal singularities (orbifolds devoid of any marginal or relevant Kähler blowup modes) and the absence of a canonical "minimal" resolution. Indeed a natural question that arises is whether terminal singularities are connected by tachyon condensation to the space of string theories. The analysis of possible endpoints in this case can be approximated by studying the condensation of the most relevant tachyon and sequentially iterating this procedure for each of the residual geometries, which are themselves typically unstable to tachyon condensation. It then turns out that the possible *final* endpoints for Type II string theories (with spacetime fermions and no bulk tachyon) cannot include terminal singularities[1] — the combinatorics combined with the constraints imposed by the GSO projection determines that there is *always* a tachyon or marginal operator in every twisted sector of a Type II orbifold. It can however be further shown that for Type 0 theories (with a bulk tachyon and no spacetime fermions), there is in fact a unique truly terminal singularity $\mathbb{C}^3/\mathbb{Z}_2\ (1,1,1)$ (resolutions are necessarily by irrelevant operators in worldsheet string theory at weak coupling) and it is included in the spectrum of endpoints of tachyon condensation.

The toric geometry description used in [9, 10] is in fact a reflection of the physics of an underlying gauged linear sigma model (GLSM) of the sort first introduced by Witten [11] as a means of studying the phases of supersymmetric Calabi-Yau spaces (and generalized to toric varieties in [12]). Explicit GLSM descriptions (and mirror descriptions) of tachyons in nonsupersymmetric orbifolds have appeared in, *e.g.*, [8, 13, 14, 15, 16, 17, 18, 19, 20].

Generically, there are multiple distinct tachyons in an unstable orbifold so that there are multiple distinct unstable channels for the decay. (More precisely, there is a continuous family of initial conditions leading to a disparate set of final decay products.) This is particularly relevant for $\mathbb{C}^3/\mathbb{Z}_N$ due to the absence of canonical "minimal" resolutions[2]: the various possible distinct resolutions are related by flip and flop transitions which are mediated by tachyonic

[1]Note, however, that *canonical* singularities (i.e., supersymmetric orbifold points) may be part of the final results of tachyon condensation.

[2]By comparison, the physics of chiral tachyon condensation dovetails beautifully with the Hirzebruch-Jung minimal resolution formulation for $\mathbb{C}^2/\mathbb{Z}_N$ [9] ensuring a unique final Kähler resolution while $\mathbb{C}/\mathbb{Z}_N$ is potentially too simple structurally to allow for distinct resolutions.

and marginal operators, respectively, in the corresponding GLSM. In this paper, we study systems of multiple tachyons and their condensation in $\mathbb{C}^3/\mathbb{Z}_N$ orbifolds using GLSM descriptions of these systems. In particular the competition between tachyons of distinct R-charges (*i.e.*, masses in spacetime) gives rise to flip transitions, described in part in [10], that relate the distinct partial resolutions of the original singularity, thought of as distinct basins of attraction for the worldsheet RG flow. A flip transition can be thought of as a blowdown of a cycle accompanied by a blowup of a topologically distinct cycle, both mediated by tachyonic (relevant) operators. Flips can always be consistently embedded in a 2-tachyon sub-GLSM (with gauge group $U(1)^2$) of the full GLSM (with gauge group say $U(1)^n,\ n \geq 2$), reflecting the fact that in the corresponding toric fan, they occur in subcones representing regions that involve "flipping" (reversing the sequence of subdivisions pertaining to) only one wall in the fan.[3] Physically a flip transition occurs for instance when a more relevant tachyon condenses during the process of condensation of a less relevant tachyon: in this case, there turn out to be interesting connections between the singularity structure of the residual endpoint geometries, the combinatorics of the toric description and the phases of the corresponding GLSM, as we will show in what follows. We show in particular that the dynamics of the GLSM RG flow always drives a flip transition in the direction of the partial resolution that leads to a less singular residual geometry, which can be thought of as a more stable endpoint. It then turns out that the phases of GLSMs corresponding to these nonsupersymmetric orbifolds can be classified into "stable" and "unstable" ones noting the directionality of the RG trajectories involving potential flip transitions, which always flow towards the more stable phases. These "stable" and "unstable" phases of GLSMs can then be identified with the corresponding extrema of the closed string tachyon potential.

The "stable" phases survive to the infrared, and provide the different basins of attraction to which the flow may tend. In many examples, there is only a single stable phase; when there are multiple stable phases, however, they are related by marginal operators in the infrared.

Organization: We first review the toric description in Sec. 1. We then describe the connections between the combinatorics, GLSMs and the singularity structure of the residual geometries in general in Sec. 2 following it up in Sec. 3 by a detailed analysis of a Type 0 example containing three tachyons. In Sec. 4, we observe that two-dimensional nonsupersymmetric orbifolds also exhibit "stable" and "unstable" phases and may also give rise to marginal operators in the infrared. We conclude in Sec. 4 with some speculations on the closed string tachyon potential.

[3]This toric operation is similar to the familiar "flop" associated to a conifold in the supersymmetric case, but it plays a different role here both physically and mathematically.

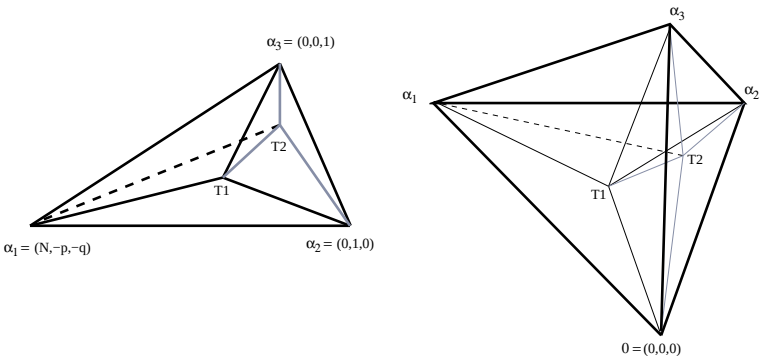

Figure 1: The fan of cones for the $\boldsymbol{N}$ lattice of $\mathbb{C}^3/\mathbb{Z}_{N(p,q)}$, with the vertices of the simplex Δ, as well as tachyons T_1, T_2 in the interior of the cone and the corresponding subdivisions. (The figure on the left shows the simplex and its subdivision; the figure on the right shows the actual cones in the fan.)

1 Review of the toric description of $\mathbb{C}^3/\mathbb{Z}_N$ tachyon condensation

In this section, we give a lightning review of the condensation of closed string tachyons localized to nonsupersymmetric noncompact $\mathbb{C}^3/\mathbb{Z}_N$ orbifold singularities, via renormalization group flows that preserve supersymmetry in the worldsheet conformal field theory and their interrelations with the combinatorial geometry of the orbifold singularities (see [10] for details). Restricting attention to $\mathcal{N} = (2,2)$ supersymmetry on the worldsheet helps us track special classes of deformations of the geometry by studying properties of the corresponding physical quantities which are protected by supersymmetry. In particular, there exist various sets of BPS-protected operators in the free conformal field theory at the orbifold point, whose operator product expansions are nonsingular: these constitute eight (anti-)chiral rings (in four conjugate pairs) in the theory for codimension three, distinguished by the choices of target space complex structure in defining the three supercurrents and $U(1)_R$ currents and therefore the superalgebra. By convention, it is the (c_X, c_Y, c_Z) ring, chiral w.r.t. the orbifold coordinates $X = z^4 + iz^5,\ Y = z^6 + iz^7,\ Z = z^8 + iz^9$, that is called the chiral ring of twisted states

$$X_j \ = \ \prod_{i=1}^{3} \ X^{(i)}_{\{jk_i/N\}} \ = \ X^{(1)}_{j/N} \ X^{(2)}_{\{jp/N\}} X^{(3)}_{\{jq/N\}}, \qquad\qquad j = 1, 2, \ldots N-1 \qquad (1)$$

constructed out of the twist fields for each of the three complex planes parametrized by X, Y, Z.

There is a remarkable correspondence between the chiral twisted sector states in the orbifold conformal field theory and the combinatorial geometry of the orbifold itself. A given orbifold

singularity can be described as a (strongly convex) rational polyhedral cone in a so-called $\boldsymbol{N}$ lattice (see figure 1): this is the lattice of divisors (codimension one algebraic subspaces) blown down at the singularity, dual to the $\boldsymbol{M}$ lattice of monomials on the orbifold space invariant under the discrete group action. Each chiral twisted state can be represented uniquely as a lattice point in the interior of this cone: *e.g.*, the twist field X_j above is the lattice point $(j, -[\frac{jp}{N}], -[\frac{jq}{N}])$ in the cone. Perturbing by a *chiral* twisted state in the orbifold conformal field theory corresponds to turning on the corresponding *Kähler* blowup mode in the geometry, *i.e.*, blowing up the corresponding divisor.

Nonsupersymmetric orbifolds in general contain twisted sector states that correspond to relevant operators on the worldsheet: these describe tachyonic instabilities in spacetime (*i.e.*, the unorbifolded dimensions) with masses

$$M^2 = \frac{4}{\alpha'}\Big(h - \frac{1}{2}\Big) < 0 \ , \tag{2}$$

where $h = \frac{|q|}{2}$ is the conformal weight with $|q| < 1$ being the R-charge of the relevant operator. Then a perturbation by such a relevant operator induces a renormalization group flow from the ultraviolet fixed point, *i.e.*, the unstable orbifold, to infrared fixed points: the divisor corresponding to the twisted state blows up giving rise to a partial resolution of the singularity. The expanding divisor locus typically contains residual singularities that are decoupled in spacetime from each other in the large radius limit, *i.e.*, the infinite RG-time limit. The combinatorics of the geometry coupled to the fact that we are restricting attention to worldsheet-supersymmetry preserving deformations enables us to follow the possible renormalization group flows all the way to their endpoints. Furthermore for Type II string theories, an appropriate GSO projection can be consistently imposed: the combinatorics along with this GSO projection is sufficient to show the nonexistence in codimension three of potential *terminal* singularities (orbifolds devoid of any blowup modes, Kähler or otherwise) thus implying that the endpoints of localized closed string tachyon condensation for Type II theories are always supersymmetric spaces[4] in codimension three as well [10], just as in the lower codimension cases [7, 8, 9]. For Type 0 theories however, the combinatorics does show the existence of a unique all-ring terminal singularity, $\mathbb{C}^3/\mathbb{Z}_2\ (1,1,1)$, which is included in the endpoints of tachyon condensation [10].

One of the new features in codimension three described in [10] was the appearance of flip transitions when multiple tachyons of differing degrees of tachyonity, *i.e.*, different worldsheet R-charges (or masses in spacetime), condense simultaneously. In such cases, there are potentially multiple basins of attraction so that in intermediate stages, distinct condensation endpoints are possible: in particular, it was found there that a more relevant tachyon gives rise

[4]That is, any remaining singularities are of the type which preserves supersymmetry.

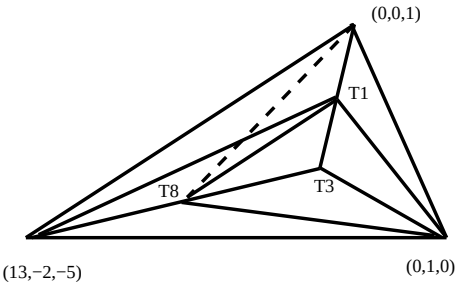

Figure 2: $\mathbb{C}^3/\mathbb{Z}_{13}$ $(1,2,5)$: The three points defining the affine hyperplane Δ of marginal operators are shown, along with the three tachyons T_1, T_3, T_8 and two distinct sequences of subdivisions. The solid lines correspond to the sequence of most relevant tachyons.

to a less singular partial resolution endpoint and vice versa. Furthermore the renormalization group trajectories corresponding to a less relevant tachyon can be forced to turn around if the more relevant tachyon turns on during this process: this turn-around behaviour is a flip transition. In this work, we describe the physics of these transitions, using explicit gauged linear sigma model constructions of the toric descriptions in [10]. These constructions allow us to study the RG flow for arbitrary initial expectation values of the condensing tachyons.

To facilitate the sections to follow, we briefly review here the toric description of an example discussed in [10] (see figure 2) which we will study in later sections using GLSMs.

Example $\mathbb{C}^3/\mathbb{Z}_{13}$ $(1,2,5)$: In the Type 0 theory, there are three tachyons T_1, T_3, T_8 in the (c_X, c_Y, c_Z) ring with R-charges $R_1 = (\frac{1}{13}, \frac{2}{13}, \frac{5}{13}) = \frac{8}{13}$, $R_3 = (\frac{3}{13}, \frac{6}{13}, \frac{2}{13}) = \frac{11}{13}$ and $R_8 = (\frac{8}{13}, \frac{3}{13}, \frac{1}{13}) = \frac{12}{13}$, respectively. The most relevant tachyon in the Type 0 theory is in fact T_1 above. In the toric fan (with vertices $\alpha_1 = (13,-2,-5)$, $\alpha_2 = (0,1,0)$, $\alpha_3 = (0,0,1)$), these tachyons correspond to the lattice vectors $T_1 = (1,0,0)$, $T_3 = (3,0,-1)$, $T_8 = (8,-1,-3)$. It is possible to show using the combinatorics of the geometry that T_1 and T_3 are coplanar with α_3 while T_3 and T_8 are coplanar with α_1. Let us first consider the subdivisions shown by the solid lines which correspond to sequentially blowing up the most relevant tachyon, *i.e.*, the sequence T_1, T_3, T_8: this gives the total $\boldsymbol{N}$ lattice volume of the subcones, *i.e.*, the degree of the residual singularity, to be $6(1)+2$. Let us consider this sequence in more detail: the first subdivision by T_1 gives the three decoupled residual geometries as the three subcones $C(0;\alpha_3,T_1,\alpha_2)$, $C(0;\alpha_1,T_1,\alpha_3)$, $C(0;\alpha_1,\alpha_2,T_1)$, which can be shown to respectively be flat space, the terminal singularity $\mathbb{Z}_2$ $(1,1,-1)$, and the supersymmetric $\mathbb{Z}_5$ $(1,2,-3)$ orbifold with marginal blowup modes (no relevant blowup modes). The renormalized R-charges of the subsequent twisted states can be shown to be $R'_3 = 1$, $R'_8 = 1$.

On the other hand, choosing a different sequence of tachyons by which to fully subdivide the cone gives rise to different fans of subcones. For instance, the dotted line in figure 2 shows the subdivision corresponding to the sequence T_3, T_8, T_1 and the corresponding flip transition. From the combinatorics, it can be shown that the subdivision by T_3 gives the subcones $C(0;\alpha_2,\alpha_3,T_3)$, $C(0;T_3,\alpha_3,\alpha_1)$ and $C(0;\alpha_1,\alpha_2,T_3)$, to be

$\mathbb{Z}_3$ $(0,1,1)$, $\mathbb{Z}_6$ $(13,-2,-3) \equiv \mathbb{Z}_6$ $(1,-2,-3)$ and $\mathbb{Z}_2$ $(-3,-6,13) \equiv \mathbb{Z}_2$ $(1,0,1)$ singularities, respectively. Further it is straightforward to show that T_8 becomes marginal after the blowup by T_3 while T_1 acquires the R-charge $R_1' = \frac{2}{3} > \frac{8}{13}$. One can now subdivide by the remaining relevant tachyons to obtain the total volume of the subcones to be $6(1)+3$: this is greater than the corresponding total volume in the most-relevant-tachyon subdivision. Thus if the tachyons T_1, T_8 condense simultaneously, then the tachyon dynamics would appear to drive the system towards the less singular endpoint, which is given by the most-relevant-tachyon sequence. In what follows, we will flesh this out in greater detail.

2 Phases of GLSMs

2.1 The condensation endpoint of a single tachyon

The condensation of a single tachyon can be modeled [8] by a gauged linear sigma model (GLSM) in two dimensions with $(2,2)$ worldsheet supersymmetry with a gauge group $U(1)$ and chiral superfields $\Psi_i \equiv \phi_1, \phi_2, \phi_3, T$. Following the conventions of [11, 12], we describe the charges under the $U(1)$ action by a charge vector

$$Q_i = (r_1, r_2, r_3, -N), \tag{3}$$

i.e., these fields transform under $U(1)$ gauge transformations as

$$\Phi_i \to e^{ir_i\lambda}\Phi_i, \qquad T \to e^{-iN\lambda}T. \tag{4}$$

The action for the GLSM (with no chiral superpotential, *i.e.*, F-terms) is

$$S = \int d^2z \, \left[d^4\theta \, \left(\bar{\Psi}_i e^{2Q_i V} \Psi_i - \frac{1}{4e^2}\bar{\Sigma}\Sigma \right) + \mathrm{Re}\Big(it \int d^2\tilde{\theta} \, \Sigma \Big) \right] , \tag{5}$$

where $t = ir + \frac{\theta}{2\pi}$, with θ the θ-angle in 1+1-dimensions and r a Fayet-Iliopoulos (FI) parameter that plays a nontrivial role in determining the vacuum structure of the theory.[5] The classical vacua of the 2D theory that preserve supersymmetry are given by solving the F- and D-term equations for the system: since there is no superpotential, there are no F-term equations, and the single D-term equation gives

$$\frac{-D}{e^2} = \sum_j q_j |\psi_j|^2 - r = \sum_{i=1}^{3} r_i |\phi_i|^2 - N|T|^2 - r = 0. \tag{6}$$

[5]Note that since the θ-angle is only determined up to multiples of 2π, the physically relevant parameter is actually $e^{2\pi i t}$. In particular, it makes sense to take $r \to \infty$, which simply sends $e^{2\pi i t}$ to 0.

Now as we vary the parameter r, the vacuum structure of the system changes. For $r \ll 0$, it is straightforward to see that this D-term equation has a solution only if the field T has nonzero vacuum expectation value. Thus, the modulus of the expectation value of the field T is fixed, and this Higgses the $U(1)$ down at low energies (relative to the scale set by e) to a residual discrete $\mathbb{Z}_N$ gauge group with generator $\omega = e^{2\pi i/N}$, as can be seen from the gauge transformations (4). This residual $\mathbb{Z}_N$ acts on the Φ_i fields as $\Phi_k \to e^{2\pi i r_k/N}\Phi_k$. The action for fluctuations of the fields Φ_i with these restricted gauge transformations in fact yields the action for a nonlinear sigma model on a $\mathbb{C}^3/\mathbb{Z}_N$ (r_1, r_2, r_3) orbifold[6] with the coordinate chart (ϕ_1, ϕ_2, ϕ_3). On the other hand, for $r \gg 0$, we can similarly see that the D-term equation admits a solution only if at least one of the fields Φ_i has a nonzero vacuum expectation value with scale $O(r)$. For instance, the D-term equation simplifies for $|\phi_i| \gg |T|$ to

$$r_1|\phi_1|^2 + r_2|\phi_2|^2 + r_3|\phi_3|^2 = r \gg 0 \tag{7}$$

which describes a weighted $\mathbb{CP}^2$ with Kähler class r in Φ-space. More generally, the D-term equation describes the divisor corresponding to the tachyonic operator in the toric description. In greater detail, in the region of moduli space where, say, $\phi_3 \neq 0$ with the other expectation values vanishing, the $U(1)$ gauge group is broken down to $\mathbb{Z}_{r_3}$, with action $\Phi_i \to e^{2\pi i r_i/r_3}\Phi_i,\ i = 1, 2,\ T \to e^{-2\pi i N/r_3}T$: the remaining massless fields yield a description of a space with the coordinate chart (ϕ_1, ϕ_2, T) characterizing the $\mathbb{C}^3/\mathbb{Z}_{r_3}$ orbifold singularity. Similarly the regions of moduli space where ϕ_1 or ϕ_2 alone acquires an expectation value yield descriptions of spaces with coordinate charts (ϕ_2, ϕ_3, T) and (ϕ_1, ϕ_3, T) characterizing $\mathbb{C}^3/\mathbb{Z}_{r_1}$ and $\mathbb{C}^3/\mathbb{Z}_{r_2}$ singularities, respectively. The regions of moduli space where multiple fields acquire expectation values describe overlaps of these coordinate charts. The collection of coordinate charts $\{\ (\phi_1, \phi_2, T),\ (\phi_2, \phi_3, T),\ (\phi_1, \phi_3, T)\ \}$ characterizes a toric variety describing the blown-up divisor with residual $\mathbb{C}^3/\mathbb{Z}_{r_i}$ singularities. The presence of $(2, 2)$ worldsheet supersymmetry ensures that the superHiggs mechanism preserves precisely the light fields required for the above geometric descriptions for each of these r values.

We see that the region $r \ll 0$ describes the unresolved $\mathbb{C}^3/\mathbb{Z}_N$ (r_1, r_2, r_3) orbifold described by coordinates represented by the fields Φ_i. The field T is the chiral primary representing the tachyon with R-charges $(\frac{r_1}{N}, \frac{r_2}{N}, \frac{r_3}{N})$: we have $R_T = \sum_i \frac{r_i}{N} < 1$ since T is tachyonic. On the other hand, the region $r \gg 0$ describes the endpoint of condensation of the tachyon T executing the partial resolution of the $\mathbb{C}^3/\mathbb{Z}_N$ (r_1, r_2, r_3) singularity, with residual $\mathbb{C}^3/\mathbb{Z}_{r_i}$ singularities. Thus the target spacetime geometry emerges as the moduli space of the GLSM in its classical phases, changing nontrivially depending on the FI parameter r in the GLSM.

[6]Ref. [20] computes the sigma model metric for $\mathbb{C}^2/\mathbb{Z}_N$ and $\mathbb{C}^3/\mathbb{Z}_N$.

The quantum story is rich. The parameter r receives 1-loop corrections

$$r \equiv r(\mu) = \sum_i Q_i \cdot \log \frac{\mu}{\Lambda} = \Big(\sum_i r_i - N\Big) \cdot \log \frac{\mu}{\Lambda} = N(R_T - 1) \cdot \log \frac{\mu}{\Lambda} \,. \tag{8}$$

This is related to a potential anomaly in the $U(1)_R$ symmetry for $\sum_i Q_i \neq 0$. In this 1-loop correction, r is renormalized to vanish at the energy scale Λ. By the usual nonrenormalization theorems of $(2,2)$ supersymmetry in two dimensions, there are no further perturbative corrections. While nonperturbative (instanton) corrections are in general present, they will be negligible for our discussions here since we will largely be concerned only with the physics of the large $|r|$ regions. There are different qualitative behaviors of the nature of quantum corrections to r, depending on the value of $\sum_i Q_i$. If $\sum_i Q_i = 0$, then there are no 1-loop corrections and r is a marginal parameter for large $|r|$. On the other hand, for a tachyonic field T with the charge vector (3), we have $\sum_i Q_i = N(R_T - 1) < 0$. Thus the 1-loop correction is nonzero and induces a renormalization group flow: r flows from the region $r \ll 0$ (orbifold phase) at high energies $\mu \gg \Lambda$, to $r \gg 0$ (partial resolution by T) at low energies $\mu \ll \Lambda$. For $\sum_i Q_i > 0$, the RG flow is reversed in direction, corresponding to an irrelevant operator.

We mention here that since the gauge coupling e in two dimensions has mass dimension one, energy scales in any physical process are defined relative to the scale set by e. Thus there are two scales in the system, e and Λ (the scale set by r), and they are independent. The full RG flow in the GLSM has two components: the first from free gauge theory (free photons) in the ultraviolet (energies much larger than the gauge coupling e) to the infrared (energies small compared to e), the second entirely in the IR, at low energies relative to e, but with nontrivial dynamics relative to the scale Λ, described in the preceding paragraph. At energies much lower than e, fluctuations transverse to the space of vacua (moduli space) cost a lot of energy. Thus the low-lying fluctuations are simply scalars defining the moduli space of the theory so that the possibility of a geometric description emerges, given by a nonlinear sigma model on the moduli space.

It is noteworthy that the RG flows in the GLSM are in principle distinct from those in the nonlinear sigma model. The *endpoints* of the RG flows in the GLSM being classical phases coincide with those of the nonlinear model and the GLSM RG flows themselves approximate the nonlinear ones in the low-energy regime $e^2 \to \infty$. The $(2,2)$-supersymmetry preserving RG flows of the GLSM can be reliably tracked in the corresponding topologically twisted A-model: the topological A-twist retains information about Kähler deformations of the model while complex structure information is in general lost. Since tachyon condensation corresponds to Kähler deformations of the orbifold, topological twisting is a sufficient tool to understand the physics of the situation. Since attention is restricted to quasi-topological observables, the gauge-coupling e^2 itself is not crucial to the discussion.

2.2 Flip transitions and N lattice volume minimization

Consider a GLSM with gauge group $U(1)\times U(1)$ and two of five chiral superfields representing tachyons T_1 and T_2 with R-charges $R_1 \equiv (\frac{a_1}{N}, \frac{b_1}{N}, \frac{c_1}{N}) = \frac{a_1}{N} + \frac{b_1}{N} + \frac{c_1}{N}$ and $R_2 \equiv (\frac{a_2}{N}, \frac{b_2}{N}, \frac{c_2}{N}) = \frac{a_2}{N} + \frac{b_2}{N} + \frac{c_2}{N}$. The action of the $U(1)\times U(1)$ on the scalar fields $\phi_1, \phi_2, \phi_3, T_1T_2$ is given by the charge matrix

$$Q_i^a = \begin{pmatrix} a_1 & b_1 & c_1 & -N & 0 \\ a_2 & b_2 & c_2 & 0 & -N \end{pmatrix}, \qquad i = 1, \ldots, 5, \quad a = 1, 2 \ . \tag{9}$$

(Such a charge matrix only specifies the $U(1)\times U(1)$ action up to a finite group, due to the possibility of a $\mathbb{Q}$-linear combination of the rows of the matrix also having integral charges.)

There are two independent FI parameters (for the two $U(1)$'s) whose variations control the vacuum structure of the theory. The classical vacua of the theory can be again found by studying the D-term equations

$$\frac{-D_i}{e^2} = a_i|\phi_1|^2 + b_i|\phi_2|^2 + c_i|\phi_3|^2 - N|T_i|^2 - r_i = 0 \ , \qquad i = 1, 2 \ . \tag{10}$$

This 2-parameter system admits several "phases" depending on the values of r_1, r_2 and we shall analyze such a system in detail in what follows. For the moment, let us focus attention on the region of moduli space where the nontrivial dynamics does not involve the field ϕ_2: in other words, we look for a linear combination of the two $U(1)$'s which does not include ϕ_2 and study the effective dynamics of this subsystem. In this case, the linear combination $b_2A_1 - b_1A_2$ of the two gauge fields can be seen to not couple to ϕ_2: the corresponding D-term is

$$\begin{aligned} \frac{-D^{eff}}{Ne^2} &= \frac{1}{N}(b_2D_1 - b_1D_2) \\ &= \frac{1}{N}(a_1b_2 - a_2b_1)|\phi_1|^2 + \frac{1}{N}(c_1b_2 - c_2b_1)|\phi_3|^2 - b_2|T_1|^2 + b_1|T_2|^2 - r^{eff}, \end{aligned} \tag{11}$$

so that the dynamics of this effective 4-field GLSM is governed by $r^{eff} = \frac{1}{N}(b_2r_1 - b_1r_2)$. The detailed physics of this system strongly depends on the combinatorics encoded by the charge matrix Q_i^a. For instance, in the example $\mathbb{C}^3/\mathbb{Z}_{13}$ $(1, 2, 5)$ studied in Sec. 3, the corresponding D^{eff}-term equation, using the charge matrix (34), is

$$\frac{-D^{eff}}{Ne^2} = |\phi_3|^2 + 2|T_2|^2 - |\phi_1|^2 - 3|T_1|^2 - r^{eff} = 0 \ . \tag{12}$$

Notice that this effective D-term has the same schematic form as that for a supersymmetric conifold exhibiting a flop[7], except that under the $U(1)$ in question here, the fields ϕ_1, ϕ_3, T_1, T_2 carry charges

$$Q_i = \begin{pmatrix} \frac{1}{N}(a_1b_2 - a_2b_1) & \frac{1}{N}(c_1b_2 - c_2b_1) & -b_2 & b_1 \end{pmatrix} \ \to \ \begin{pmatrix} 1 & 2 & -1 & -3 \end{pmatrix} \ , \tag{13}$$

[7]Recall that a supersymmetric conifold can be expressed as a hypersurface in $\mathbb{C}^4$: then in terms of a $U(1)$

so that $\sum_i Q_i \neq 0$. This is a reflection of tachyons at play, giving an inherent directionality to the dynamics. This is a nonsupersymmetric analogue of a conifold region, with nontrivial dynamics in time. We can study the phases of this effective 4-field GLSM along the same lines as the previous section, and along the same lines as for the flop described *e.g.*, in [11] [5].
For $r^{eff} \ll 0$, we have $|\phi_1|^2 + 3|T_1|^2 \sim -r^{eff}$, describing a $\mathbb{P}^1_-$ with residual singularities described by the coordinate charts (ϕ_3, T_2, ϕ_1), (ϕ_3, T_2, T_1). For $r^{eff} \gg 0$, we have $|\phi_3|^2 + 2|T_2|^2 \sim r^{eff}$, describing a $\mathbb{P}^1_+$ with residual singularities described by the coordinate charts (ϕ_3, ϕ_1, T_1), (T_2, ϕ_1, T_1).

Now from the 1-loop running of the FI parameters, we have

$$r_1(\mu) = N(R_1 - 1) \cdot \log \frac{\mu}{\Lambda}, \qquad r_2(\mu) = N(R_2 - 1) \cdot \log \frac{\mu}{\Lambda}, \tag{14}$$

so that the 1-loop running of r^{eff} is

$$r^{eff} = \Big[\Big(\frac{a_1}{N} + \frac{c_1}{N} - 1\Big)b_2 - \Big(\frac{a_2}{N} + \frac{c_2}{N} - 1\Big)b_1\Big] \cdot \log \frac{\mu}{\Lambda} \;\rightarrow\; (-1)\, \log \frac{\mu}{\Lambda}\ . \tag{15}$$

Thus r^{eff} flows under the renormalization group from the $r^{eff} \ll 0$ phase (partial resolution by $\mathbb{P}^1_-$) to the $r^{eff} \gg 0$ phase (partial resolution by $\mathbb{P}^1_+$). This is the GLSM reflection of the flip transition in spacetime – clearly it involves the blowdown of the 2-cycle $\mathbb{P}^1_-$ followed by a blowup of the topologically distinct $\mathbb{P}^1_+$. To understand the significance of the coefficient of the logarithm in (15), it is helpful to revisit the toric description of the orbifold decay [10] and the corresponding flip region. Condensation of a localized tachyon gives rise to an expanding bubble (containing a divisor) with three decoupled regions which can potentially contain residual singularities. We now review the relation [10] between the relevance (R-charges) of distinct tachyons and the $\boldsymbol{N}$ lattice volumes of the subcones (which effectively gives the cumulative order or degree of the residual singularities) resulting from the subdivisions corresponding to those tachyons. Let us begin with the cone $C(0; \alpha_1, \alpha_2, \alpha_3)$ corresponding to the unresolved $\mathbb{C}^3/\mathbb{Z}_{N(p,q)}$ singularity (see figure 1). Now add a lattice point $T_j = (j, -[\frac{jp}{N}], -[\frac{jq}{N}])$ corresponding to a tachyon T_j. Then the total $\boldsymbol{N}$ lattice volume of the three residual subcones after subdivision with the tachyon T_j is easily calculated: let $V(e_0; e_1, e_2, e_3)$ denote the volume of a cone subtended by the vectors e_1, e_2, e_3 with the vector e_0 being the apex. Then (see, *e.g.*,

GLSM with fields z_1, z_2, z_3, z_4 carrying charges $(+1, +1, -1, -1)$, respectively, under the $U(1)$, the corresponding D-term is

$$\frac{-D^{flop}}{e^2} \;=\; |z_1|^2 + |z_2|^2 - |z_3|^2 - |z_4|^2 - \rho\ .$$

The conifold singularity itself is at $\rho = 0$ classically. Redefining the variables z_i can be used to recast the above equation in perhaps more familiar forms.

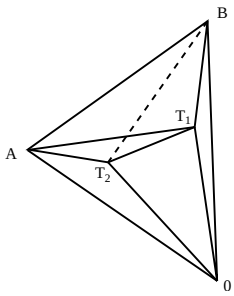

Figure 3: A flip region in the toric fan for $\mathbb{C}^3/\mathbb{Z}_{13}$ $(1,2,5)$ defined by the convex hull $\{A, B, T_1, T_2\}$. The solid lines show the subdivision for the sequence T_1, T_2 giving smaller $\boldsymbol{N}$ lattice volume while the dotted line shows the subdivision for the reversed sequence.

figure 1) we have

$$V_{subcones}(T_j) = V(0; \alpha_1, \alpha_2, \alpha_3) - V(T_j; \alpha_1, \alpha_2, \alpha_3) = NR_j < N \ , \tag{16}$$

where the volume of a cone $V(0; e_1, e_2, e_3) = |\det(e_1, e_2, e_3)| = |e_1 \cdot (e_2 \times e_3)|$. Now if we consider two tachyons T_1 and T_2 (as in figure 1), such that T_1 is more relevant than T_2, *i.e.*, $R_1 < R_2$, where $R_i = \frac{j_i}{N} + \{\frac{j_i p}{N}\} + \{\frac{j_i q}{N}\}$, this implies $V_{subcones}(T_1) < V_{subcones}(T_2)$. Thus given an orbifold singularity, isolated condensation of a more relevant tachyon locally leads to a less singular partial resolution. Now if both tachyons simultaneously condense, then the toric description shows the existence of a region exhibiting a flip transition. For instance, in $\mathbb{C}^3/\mathbb{Z}_{13}$ $(1,2,5)$, the region in question is given by the convex hull subtended by the $\boldsymbol{N}$ lattice points $\alpha_1, T_8, T_1, \alpha_3$ with the origin $(0,0,0)$ (see figure (2)). The most-relevant-tachyon sequence T_1, T_8, T_3 (*i.e.*, the subdivision given by the solid lines) results in a less singular endpoint geometry than, say, the sequence T_8, T_1, T_3. In the general case we describe above, the corresponding flip region is the convex hull subtended by the $\boldsymbol{N}$ lattice points $A \equiv (N, -p, -q)$, $B \equiv (0,0,1)$, $T_1 \equiv (j_1, -[\frac{j_1 p}{N}], -[\frac{j_1 q}{N}])$, $T_2 \equiv (j_2, -[\frac{j_2 p}{N}], -[\frac{j_2 q}{N}])$ with the origin $0 \equiv (0,0,0)$, as shown in figure 3. We can calculate the difference in the $\boldsymbol{N}$ lattice volumes of the corresponding subcones to get a quantitative measure of the difference in the degree of singularity between the two blowup sequences as

$$\Delta V = V(0; A, T_1, B) + V(0; A, T_2, T_1) - V(0; B, T_2, T_1) + V(0; A, T_2, B) \ . \tag{17}$$

Using the coordinate values for the lattice points, the expression above can be simplified to give

$$\Delta V = \Big(\frac{j_1}{N} + \Big\{\frac{j_1 q}{N}\Big\} - 1\Big)\, N\Big\{\frac{j_2 p}{N}\Big\} - \Big(\frac{j_2}{N} + \Big\{\frac{j_2 q}{N}\Big\} - 1\Big)\, N\Big\{\frac{j_1 p}{N}\Big\} \ . \tag{18}$$

By rewriting this expression in terms of the R-charges (a_i, b_i, c_i) for the tachyons T_1, T_2, it is straightforward to recognize (see eqn.(15)) that this is precisely the coefficient of the logarithm in r^{eff}, *i.e.*,

$$r^{eff} = (\Delta V) \cdot \log \frac{\mu}{\Lambda} \ . \tag{19}$$

Thus the RG flow for this effective FI parameter proceeds precisely in the direction of decreasing $\boldsymbol{N}$ lattice volume, *i.e.*, in the direction along which $\Delta V < 0$. In other words, the renormalization group dynamics in the GLSM drives the flip transition in the direction of the partial resolution that leads to a less singular residual geometry, which can be thought of as a stable endpoint of this effective RG flow.

If the tachyon T_1 is more relevant than T_2, then we have $R_1 < R_2$: the 1-loop coefficient in the FI parameter for a given tachyon is related to its R-charge. As we have seen, when the tachyons condense individually, the cumulative volume of the residual singularities is smaller for T_1, in other words, the more relevant tachyon leads to a less singular endpoint and vice versa. What the above calculation shows is that when two tachyons condense simultaneously, the 1-loop coefficient in the relative FI parameter r^{eff} is related to the difference in the degrees of the residual singularities, *i.e.*, the $\boldsymbol{N}$ lattice volume difference between the two toric subdivisions performed in either of the two possible orders.

2.3 The n-tachyon system: some generalities

We will now describe some generalities[8] on closed string tachyon condensation in an unstable orbifold with multiple tachyons via gauged linear sigma models[9]. The action for a GLSM for a target space $\mathbb{C}^d/\mathbb{Z}_N$ can be written as

$$S = \int d^2z \ \Big[d^4\theta \ \Big(\bar{\Psi}_i e^{2Q_i^a V_a} \Psi_i - \frac{1}{4e_a^2} \bar{\Sigma}_a \Sigma_a \Big) + \mathrm{Re}\Big(it_a \int d^2\tilde{\theta} \ \Sigma_a \Big) \Big] \ , \tag{20}$$

where summation on the index $a = 1, \ldots, n$ is implied. The $t_a = ir_a + \frac{\theta_a}{2\pi}$ are Fayet-Iliopoulos parameters and θ-angles for each of the n gauge fields. The twisted chiral superfields Σ_a (whose bosonic components are complex scalars σ_a) represent field-strengths for the gauge fields. The various chiral superfields $\Psi_i, \ i = 1, \ldots, d+n$ in the GLSM are the d coordinate superfields Φ_i

[8] Due to the possibly technical nature of this subsection, it might be useful to read this in conjunction with the next section which elucidates these generalities in a specific example.

[9] We continue to use conventions of [11, 12].

and the n tachyons T_k : for $d = 3$, the action of the $U(1)^n$ gauge group on them is given as

$$\Psi_i \to e^{iQ_i^a\lambda}\ \Psi_i\ , \qquad Q_i^a = \begin{pmatrix} q_1^1 & q_2^1 & q_3^1 & -N & 0 & \dots \\ q_1^2 & q_2^2 & q_3^2 & 0 & -N & \dots \\ & & \cdot & & & \dots \\ & & \cdot & & & \dots \end{pmatrix}, \qquad a = 1, \dots, n \tag{21}$$

where Q_i^a is the $n \times (d+n)$ charge matrix (although in order to accurately specify the group action, some of these rows may need to replaced by $\mathbb{Q}$-linear combinations of the original rows). From the point of view of the target spacetime, this gives the R-charges of the n tachyons to be $R_a \equiv (\frac{q_1^a}{N}, \frac{q_2^a}{N}, \frac{q_3^a}{N}) = \sum_{i=1}^3 \frac{q_i^a}{N}$, $a = 1, \dots, n$. The theory described by this GLSM is super-renormalizable: the only divergence arises in the 1-loop renormalization of the n Fayet-Iliopoulos parameters, given by

$$r_a = \Big(\sum_i Q_i^a \Big) \cdot \log \frac{\mu}{\Lambda}\ , \tag{22}$$

where μ is the RG scale and Λ is an ultraviolet cutoff scale where the r_a are defined to vanish. Thus all RG flowlines in r-space are straight lines at the level of these 1-loop equations. In general there may be nonperturbative (instanton) corrections to the theory in the small r regions, which are expected to transform these straight flowlines into curves: for our purposes here, we will not need to consider these since we will only be interested in the phases of the GLSM for large r. If we consider GLSMs with strictly relevant operators, we have $\sum_i Q_i^a < 0$ for all $a = 1, \dots, n$: then the GLSM renormalization group drives the system towards the region where all of the $r_a > 0$.

The space of classical ground states of this theory can be found by the bosonic potential

$$U = \sum_{a=1}^n \frac{(D_a)^2}{2e_a^2} + 2 \sum_{a,b=1}^n \bar\sigma_a \sigma_b \sum_{i=1}^{n+d} Q_i^a Q_i^b |\phi_i|^2\ . \tag{23}$$

Then $U = 0$ requires $D_a = 0$: solving these for $r_a = 0$ gives expectation values for the ϕ_i which Higgs the $U(1)^n$ down to Z_N and lead to mass terms for the σ_a whose expectation values thus vanish. The classical phase diagram of the GLSM is then given in terms of solutions to the D-term equations

$$-\frac{D_a}{e_a^2} = \sum_{i=1}^{d+n} Q_i^a |\psi_i|^2 - r_a = 0\ , \qquad a = 1, \dots, n\ . \tag{24}$$

These give collections of coordinate charts that characterize in general distinct toric varieties, depending on the n FI parameters r_a. In other words, as we vary r_a we pass through several distinct "phases" [11] in r-space that represent in general distinct target space geometries. The

explicit description of these toric varieties is a standard exercise in toric geometry, which we now review.

We have studied the 2-tachyon $\mathbb{C}^3/\mathbb{Z}_N$ system in the previous subsection on flip transitions and will study it in greater detail later. Specialize now to $\mathbb{C}^3/\mathbb{Z}_N$ and $n > 2$: then we find in r-space (which is n-dimensional here) several distinct phase bounding n-vectors $\phi_1 \equiv (q_1^1, q_1^2, \ldots),\ \phi_2 \equiv (q_2^1, q_2^2, \ldots),\ \phi_3 \equiv (q_1^3, q_3^2, \ldots),\ \ T_1 \equiv (-N, 0, \ldots),\ T_2 \equiv (0, -N, \ldots),\ \ldots$: these can be read off as the $3+n$ columns in the charge matrix (21). Hyperplanes of various dimensionalities embedded in r-space subtended by these phase bounding vectors give rise to phase boundaries. At the location of such a phase boundary, some (but not all) of the r_a vanish thus giving rise to singularities classically. These hyperplanes defining phase boundaries intersect along rays emanating from the origin in r-space. The set of these intersection rays includes the $3+n$ vectors $\psi_i \equiv \phi_i, T_j$ but also in general contains new vectors $\{\phi_{Int}\}$. Each classical phase of the GLSM is thus an n-dimensional convex hull (or n-simplex) in r-space, *i.e.*, the interior region of n-tuples of the full set of intersection rays $\{\phi_i, T_j, \phi_{Int}\}$. We can gain insight into the geometric structure of r-space by gleaning the geometric relations amongst the intersection rays, effectively treating them as toric data and studying their combinatorics: doing so results in the *secondary fan* of the system.

Note that a given convex hull may itself be contained in other convex hulls: thus a given region in r-space typically admits more than simply one description on the moduli space of the GLSM in terms of coordinate charts in spacetime. Thus each convex hull or phase (which is a well-defined region in r-space) yields a collection of coordinate charts in general (rather than a single chart), which then describes a toric variety in spacetime.

It is important to note that k-tachyon subsystems of this n-tachyon system can be studied consistently independent of the other $n-k$ tachyons by taking appropriate limits of the original GLSM. The moduli space of the GLSM for the subsystem is given as the subspace obtained by restricting to $r_\ell \to -\infty,\ \ell = k+1, \ldots, n-k$. This decoupling of the $n-k$ tachyons is consistent, showing that condensation of some of the tachyons does not source the remaining ones[10]: we will have more to say on this later when we describe in detail the stability of the phases of the GLSM in a specific example.

It is convenient to choose a basis for Q_i^a such that $a = 1$ represents the most relevant tachyon. Then we have $R_1 \leq R_b,\ b \neq 1$ so that $|\sum_i Q_i^1| = |N(R_1 - 1)| \geq |\sum_i Q_i^b|,\ b \neq 1$. A generic linear combination of the n $U(1)$ gauge fields in this theory couples to a linear

[10]This is consistent with the results of [24] for $\mathbb{C}/\mathbb{Z}_N$ who compute off-shell correlators for various tachyons (twisted states) and find that the cubic interaction vanishes within their approximations, showing that condensation of one tachyon does not source others.

combination of the n FI parameters, which then has the 1-loop renormalization

$$r_\alpha = \Big(\sum_{\alpha=1}^{n} \alpha_a \sum_{i=1}^{n+d} Q_i^a\Big) \cdot \log\frac{\mu}{\Lambda} \ , \tag{25}$$

the α_a being arbitrary real numbers. The above linear combination of the $U(1)$'s is marginal if the coefficient of r_α vanishes, *i.e.*,

$$\sum_{\alpha=1}^{n}\sum_{i=1}^{n+d} \alpha_a Q_i^a = 0 \ . \tag{26}$$

This equation defines a codimension-one hyperplane perpendicular to a ray emanating from the origin and passing through the point $(-\sum_i Q_i^1, -\sum_i Q_i^2, \ldots, -\sum_i Q_i^n)$ in r-space which has real dimension n. This point lies in the $r_a > 0$ region of r-space for GLSMs containing only tachyonic operators[11]—we henceforth call this the *flow-ray*.

We can redefine the charge matrix Q_i^a in a useful way that will help illustrate some of the physics of the orbifold decay in general. Define

$$Q_i^{a\prime} \equiv \Big(\sum_i Q_i^1\Big) Q_i^a - \Big(\sum_i Q_i^a\Big) Q_i^1 \ , \qquad\qquad a \neq 1 \ . \tag{27}$$

In other words, we have, *e.g.*, $Q_1^{2\prime} = N(R_1 - 1)q_1^2 - N(R_2 - 1)q_1^1$. With this redefinition, we have $\sum_i Q_i^{a\prime} = (\sum_i Q_i^1)(\sum_i Q_i^a) - (\sum_i Q_i^a)(\sum_i Q_i^1) = 0$, for $a \neq 1$, so that the FI parameters coupling to these redefined $n-1$ gauge fields have vanishing 1-loop running. Thus there is a single relevant direction (along the flow-ray) and $n-1$ marginal directions in r-space.

Since the FI parameters r_a necessarily are renormalized, we expect from the structure of the RG flowlines in r-space that some phases will represent *stable* fixed points while others will be *unstable* (in the sense of the renormalization group) and will flow to the stable ones. Thus we expect that the geometry, in a given initial phase, is in general forced to dynamically evolve to another, more stable, phase, possibly passing through intermediate phases: this potential instability and the decay to a stable endpoint geometry is the spacetime reflection of the renormalization group running of the FI parameters in the GLSM. By studying various linear combinations (25), we see that the 1-loop renormalization group flows drive the system along the single relevant direction to the phases in the large r regions of r-space, *i.e.*, $r_a \gg 0$, that are adjacent to the flow-ray $f \equiv (-\sum_i Q_i^1, -\sum_i Q_i^2, \ldots, -\sum_i Q_i^n)$, or contain it in their interior.

[11] Recall that for appropriate isolated nonsupersymmetric orbifolds $\mathbb{C}^3/\mathbb{Z}_N$ $(1,p,q)$, there are no marginal twisted sector states, only tachyons (and of course irrelevant operators).

The spacetime reflection of the single relevant (tachyonic) direction in r-space is the existence of a dominant unstable direction for the decay of the orbifold. The $n-1$ marginal directions of the GLSM perpendicular to the flow-ray indicate the presence of $n-1$ flat directions (moduli) of the tachyon potential in spacetime. These flat directions are in general appropriate combinations of the subsequent tachyonic twisted states besides the dominant (most relevant) tachyon. In the example $\mathbb{C}^3/\mathbb{Z}_{13}$ $(1,2,5)$ that we discuss in detail in Sec. 3, there are three twisted sector tachyons: the combinatorics of Q_i^a determines that the two residual flat directions are in fact the two subsequent twisted states themselves, besides the most relevant tachyon T_1, *i.e.*, the subsequent tachyons get renormalized under the RG flow induced by T_1 and become marginal.

Note that even if all r_a are initially large, some of them may become small during RG flow, rendering our semiclassical analysis untrustworthy. However, for inital values of r_a whose components in the marginal directions lie far from the center of the marginal $(n-1)$-plane, the values of r_a remain large throughout the RG flow.

The combinatorial geometry of the flow-ray in r-space determines the physical structure of the tachyon potential. In particular, the combinatorics of the charge matrix Q_i^a determines whether the flow-ray is in the interior of all possible convex hulls of n-tuples of vectors in r-space or an edge to one or more of them. For instance, consider a 2-tachyon system (see figure 1) where a subsequent tachyon, say T_2, is marginal, *i.e.*,

$$R_2' = R_2 \left(1 + \frac{q_1^2}{q_1^1}\frac{1-R_1}{R_2}\right) = 1 \ , \tag{28}$$

using the results of [10] for the renormalized R-charges of subsequent tachyons. This can be simplified and used to show that $q_1^2 \sum_i Q_i^1 = q_1^1 \sum_i Q_i^2$, which therefore implies that the flow-ray $f \equiv (-\sum_i Q_i^1, -\sum_i Q_i^2) \propto (q_1^1, q_1^2) \equiv \phi_1$, using (9), (21). This shows that the flow-ray f is the phase boundary ϕ_1 and therefore an edge to two or more convex hulls, *i.e.*, it is not in the interior of all convex hulls. Therefore we conclude that the flow-ray is the phase boundary between two distinct phases that are connected by the single marginal direction perpendicular to the flow-ray f. We can get additional insight into the structure of these phases: for instance if $\frac{q_2^2}{q_2^1} > \frac{q_1^2}{q_1^1} = \frac{\sum_i Q_i^2}{\sum_i Q_i^1}$, then we have $q_2^2 \sum_i Q_i^1 - q_2^1 \sum_i Q_i^2 > 0$, giving the direction of the flip transition of the previous subsection. Note that a flip region such as the one described in the previous subsection can always be embedded in a 2-tachyon subsystem of the n-tachyon system since the flip transition always involves flipping only one "wall" in the toric fan. Such an embedding provides useful information about the transition (although the 2-tachyon subsystem may not completely decouple from the other tachyons, so this information must be used with care.)

We will now describe quantum corrections to the classical r-space. The discussion here is applicable away from the region in r-space where not all of the r_a are small (*i.e.*, for r-values far from the origin in r-space). The 1-loop renormalization of the FI parameters can be expressed [11, 5, 12] as a σ-dependent shift in terms of a perturbatively quantum-corrected twisted chiral superpotential for the Σ_a

$$\tilde{W}(\Sigma) = \frac{1}{2\sqrt{2}} \sum_{a=1}^{n} \Sigma_a \Big(i\hat{\tau}_a - \frac{1}{2\pi} \sum_{i=1}^{d+n} Q_i^a \log(\sqrt{2} \sum_{b=1}^{n} Q_i^b \Sigma_b/\Lambda) \Big) \ . \tag{29}$$

This expression has been obtained by considering the large-σ region in field space and integrating out those scalars ψ_i that are massive here (and their expectation values vanish energetically). This leads to a modification in the potential energy

$$U(\sigma) = \frac{e^2}{2} \sum_{a=1}^{n} \Big| i\hat{\tau}_a - \frac{\sum_{i=1}^{d+n} Q_i^a}{2\pi} (\log(\sqrt{2} \sum_{b=1}^{n} Q_i^b \sigma_b/\Lambda) + 1) \Big|^2 \ . \tag{30}$$

The singularities predicted classically at the locations of the phase boundary hyperplanes arise from the existence of low-energy states at large σ. Now from above, we see that along the single relevant direction where $\sum_i Q_i^1 \neq 0$, the potential energy has a $|\log(\sigma_1)|^2$ growth so that the field space accessible to very low-lying states is effectively compact and there is no singularity along the single relevant direction given by the flow-ray: in other words, the RG flow is smooth along the tachyonic directions for all values of τ_1. Thus a phase boundary hyperplane that was a singularity classically is simply a label for the boundary of the adjacent phases quantum mechanically. Continuing past this non-existent "singularity" to a region where r_1 differs in sign from $\sum_i Q_i$, we find σ-vacua at large $|r_1|$. These nonclassical Coulomb branch vacua are also possible IR endpoints of the RG flows of the GLSM along with the geometric endpoints on the Higgs branch: thus tachyon condensation drives an unstable orbifold generically to a combination of the geometric Higgs branch vacua and nonclassical Coulomb branch vacua. The Higgs branch vacua have a transparent interpretation in terms of the partial resolutions of the orbifold geometry and are thus describable in principle in terms of the nonlinear sigma models describing the orbifold. The nonclassical Coulomb branch vacua, crucial in ensuring that quasi-topological quantities such as the number of vacua are preserved along the RG flow [15], should also in principle be visible from the nonlinear sigma model point of view: it would be interesting to investigate this question more directly.

On the other hand, along the $n-1$ marginal directions, we have $\sum_i Q_i^{b'} = 0, \ b \neq 1$: then there are simply constant shifts

$$\tau_b^{eff\,\prime} = \tau_b{}' + \frac{i}{2\pi} \sum_{i=1}^{n} Q_i^{b'} \log(Q_i^{b'}) \ , \tag{31}$$

which is σ-independent (note that this is valid only in the vicinity of one r_i small and all other r_a large). There is a singularity for $\tau_b^{eff'} = 0$, which exists for a particular value of r_b and θ_b, in other words for complex codimension one. Thus the distinct phases can be continuously connected by paths in r-space lying in the marginal hyperplane since we have the freedom of turning on a nonzero θ-angle distinct from the singular value.

The extrema of the quantum-corrected superpotential (29) are given by

$$\prod_{i=1}^{d+n} \Big(\frac{\sqrt{2}e}{\Lambda} \sum_{b=1}^{n} Q_i^b \sigma_b \Big)^{Q_i^a} = e^{2\pi i \tau_a} \equiv q_a \ , \qquad a = 1, \ldots, n \ . \tag{32}$$

These inhomogeneous equations for the σ_a can be recast using the redefined charges $Q_i^{a'}$ given in (27) and redefining the σ_a in terms of appropriate linear combinations to obtain one inhomogeneous equation for the single relevant $U(1)$ (which is the corresponding equation for $a = 1$ above) and $n-1$ homogeneous equations for the marginal $U(1)$'s

$$\prod_{i=1}^{d+n} \Big(\sum_{b=2}^{n} Q_i^{b'} \sigma'_b \Big)^{Q_i^{a'}} = e^{2\pi i \tau'_a} \equiv q'_a \ , \qquad a = 2, \ldots, n \ . \tag{33}$$

Notice that the cutoff Λ, which is the signature of the RG flow, does not appear in these equations as expected, since these contain only marginal directions. These equations contain nontrivial information about the nonclassical large-σ Coulomb branch vacua that exist at the infrared of the RG flow, at large r_a.

3 Phases of a GLSM: $\mathbb{C}^3/\mathbb{Z}_{13}$ $(1,2,5)$

In what follows, we will flesh out the above phenomena in detail in a specific example: we will describe the Type 0 string theory on the unstable nonsupersymmetric orbifold $\mathbb{C}^3/\mathbb{Z}_{13}$ $(1,2,5)$ studied in [10] via toric methods (and reviewed in Sec. 1). Appropriate GSO projections can be imposed without changing the essential points of our discussion here. We restrict attention to the three tachyons arising in the (c_X, c_Y, c_Z) ring of twisted states of the orbifold: this is equivalent to performing a topological twist that retains only the chiral (c_X, c_Y, c_Z) ring, projecting out the remainder.

3.1 The 2-parameter system: two tachyons

The classical phase diagram

In this subsection (see also Sec. 2.2), we will ignore the tachyon T_3 for simplicity and focus on the physics of the condensation of tachyons T_1 and T_8: this gives a GLSM with gauge group

$U(1)\times U(1)$ whose physics is consistent with the full three-tachyon analysis of the $U(1)^3$ GLSM we do in a later subsection. The tachyons T_1 and T_8 have R-charges $R_1 \equiv (\frac{1}{13}, \frac{2}{13}, \frac{5}{13}) = \frac{8}{13}$ and $R_8 \equiv (\frac{8}{13}, \frac{3}{13}, \frac{1}{13}) = \frac{12}{13}$. The vacuum structure of the theory is governed by two independent FI parameters coupling to the two $U(1)$'s: these parameters run under the RG flow induced by the two tachyonic operators in the GLSM. The action of the $U(1) \times U(1)$ on the fields $\Psi_i \equiv \phi_1, \phi_2, \phi_3, T_1, T_8$ is given, as in (21), by $\Psi_i \to e^{iQ_i^a \lambda}\ \Psi_i$, where the charge matrix is

$$Q_i^a = \begin{pmatrix} 1 & 2 & 5 & -13 & 0 \\ 8 & 3 & 1 & 0 & -13 \end{pmatrix}. \tag{34}$$

(We shall use this version of the charge matrix which makes the tachyons visible, but a more accurate version would replace the first row by

$$\begin{pmatrix} 3 & 1 & 0 & 1 & -5 \end{pmatrix}, \tag{35}$$

which is $-\frac{1}{13}$ times the first row plus $\frac{5}{13}$ times the second.)

The classical vacua of the theory, *i.e.*, the phase diagram of the corresponding GLSM, are found by studying the D-terms

$$\begin{aligned} D_1 &= |\phi_1|^2 + 2|\phi_2|^2 + 5|\phi_3|^2 - 13|T_1|^2 - r_1 = 0, \\ D_2 &= 8|\phi_1|^2 + 3|\phi_2|^2 + |\phi_3|^2 - 13|T_8|^2 - r_2 = 0. \end{aligned} \tag{36}$$

In the region $r_1, r_2 \ll 0$, nonzero vacuum expectation values are forced upon both T_1 and T_8: these break the $U(1) \times U(1)$ down to a discrete group $\mathbb{Z}_{13}$ with generator $\omega = e^{2\pi i/13}$, whose action on the coordinate fields ϕ_i is given by $g : (\phi_1, \phi_2, \phi_3) \to (\omega\phi_1, \omega^2\phi_2, \omega^5\phi_3)$. This is thus the unresolved $\mathbb{C}^3/\mathbb{Z}_{13}$ $(1, 2, 5)$ orbifold phase. In this phase, the point $\{T_1 = 0\ \cup\ T_8 = 0\}$ must be excluded from the moduli space since there is no solution to the D-term equations at that point: this point is the excluded set in this phase.

Now the various other phases can be obtained by focussing on different linear combinations of the two $U(1)$'s and realizing the D-terms for them, and thereby the phases. The linear combinations

$$\begin{aligned} D_1' &= \frac{1}{13}(8D_1 - D_2) = |\phi_2|^2 + 3|\phi_3|^2 - 8|T_1|^2 + |T_8|^2 - \frac{8r_1 - r_2}{13} = 0, \\ D_2' &= \frac{1}{13}(3D_1 - 2D_2) = -|\phi_1|^2 + |\phi_3|^2 - 3|T_1|^2 + 2|T_8|^2 - \frac{3r_1 - 2r_2}{13} = 0, \\ D_3' &= \frac{1}{13}(-D_1 + 5D_2) = 3|\phi_1|^2 + |\phi_2|^2 + |T_1|^2 - 5|T_8|^2 + \frac{r_1 - 5r_2}{13} = 0, \end{aligned} \tag{37}$$

show that the rays drawn from the origin $(0, 0)$ out to $(1, 8), (2, 3), (5, 1)$ are phase boundaries, alongwith the rays $(-13, 0), (0, -13)$ gleaned from (36).

To illustrate how the moduli space of the GLSM realizes these phases, let us study, for instance, the convex hull defined by the rays $(2,3)$ and $(5,1)$ (see Figure 4): then we have $3r_1 - 2r_2 \gg 0,\ -r_1 + 5r_2 \gg 0$, *i.e.*, $\frac{1}{5}r_1 < r_2 < \frac{3}{2}r_1$, which automatically implies $r_1,\ r_2,\ -r_1 + 8r_2 \gg 0$. Then solutions to D_2' and D_3' exist if at least one of $\{\phi_3, T_8\}$ and $\{\phi_1, \phi_2, T_1\}$ have nonzero expectation values. Consider the region of moduli space where ϕ_3 and ϕ_2 alone acquire expectation values: then at low energies, the remaining massless fields are ϕ_1, T_1, T_8 which yield a description of the coordinate chart (ϕ_1, T_1, T_8). Note that this is compatible with the constraints given by D_1, D_2, D_1'. Likewise, the region of moduli space where ϕ_3 and ϕ_1 alone acquire expectation values leaves the remaining massless fields describing the coordinate chart (ϕ_2, T_1, T_8). Similarly, the regions where ϕ_3, T_1 or T_8, ϕ_1 or T_8, ϕ_2 alone acquire expectation values yield descriptions of spaces with coordinate charts (ϕ_1, ϕ_2, T_8), (ϕ_2, ϕ_3, T_1) and (ϕ_1, ϕ_3, T_1), respectively[12]. If multiple fields acquire nonzero expectation values, the remaining massless fields describe overlaps of some of these coordinate charts obtained above. Thus the convex hull defined by rays $(2,3)$ and $(5,1)$ admits a description of the spacetime geometry by the collection of coordinate charts $\{\ (\phi_1, T_1, T_8),\ (\phi_2, T_1, T_8),\ (\phi_1, \phi_2, T_8),\ (\phi_2, \phi_3, T_1),\ (\phi_1, \phi_3, T_1)\ \}$. From Figure 2, we see that this collection of charts describes the complete resolution of the orbifold obtained by the condensation of tachyons T_1 and T_8 in that sequence: recall that this is the most relevant tachyon sequence which leads to the least singular residual spacetime geometry.

By a similar analysis of the D-term equations, we can get a physical understanding of the geometry described in each of the other phases of the GLSM.

A simple operational method[13] to realize the results of the above analysis of the D-terms for the phase boundaries and the phases of the GLSM is the following: read off each column from the charge matrix Q_i^a (eqn.(34)) as a ray emanating outwards from the origin $(0,0)$ in (r_1, r_2)-space, representing a phase boundary. Then the various phases in this 2-parameter system are simply given by the convex hulls bounded by any two of the (in this case, five) phase boundaries represented by the rays $\phi_1 \equiv (1,8),\ \phi_2 \equiv (2,3),\ \phi_3 \equiv (5,1),\ T_1 \equiv (-13,0),\ T_8 \equiv (0,-13)$. These phase boundaries divide the (r_1, r_2)-plane into five phase regions. There are several possible overlapping coordinate charts characterizing any given phase of these five described as a convex hull of two phase boundaries: these can be read off by noting all the possible convex

[12]Following this logic would lead one to suspect the existence of a region in moduli space for this phase in r-space where T_1, T_8 alone acquire expectation values: however from D_1', D_2', D_3', we obtain conditions $|T_8|^2 \gg 8|T_1|^2,\ |T_8|^2 \gg \frac{3}{2}|T_1|^2,\ |T_1|^2 \gg 5|T_8|^2$, which do not admit any solution thus precluding the existence of the corresponding chart.

[13]We mention here for convenience that a 2-dim convex hull is defined as the interior of a region bounded by two rays emanating out from the origin such that the angle subtended by them is less than π.

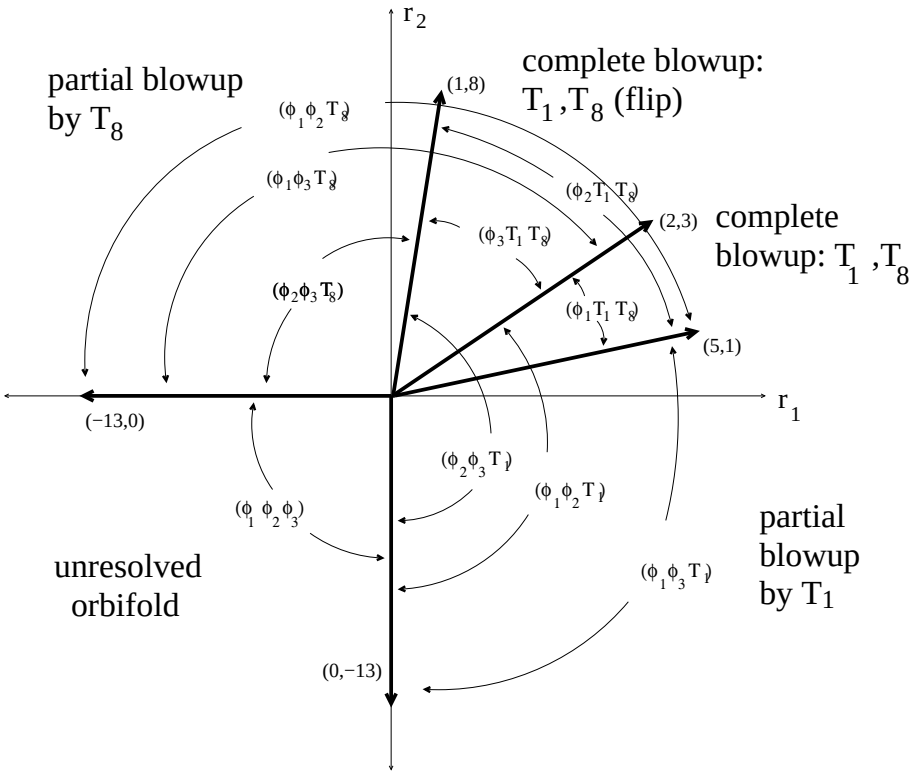

Figure 4: Phases of $\mathbb{C}^3/\mathbb{Z}_{13}$ $(1,2,5)$: the 2-parameter system of the two tachyons T_1, T_8. Also shown are the various coordinate charts characterizing each of the five phases.

hulls that contain the convex hull (phase) in question.

For instance, consider the convex hull $\{\phi_2, \phi_3\}$: this is also contained in the convex hulls $\{\phi_1, \phi_3\}$, $\{T_1, \phi_3\}$, $\{\phi_2, T_8\}$ and $\{\phi_1, T_8\}$. The coordinate chart describing a particular convex hull, say $\{\phi_2, \phi_3\}$ is read off as the complementary set $\{\phi_1, T_1, T_8\}$. Thus the full set of coordinate charts characterizing the toric variety in the phase given by the convex hull $\{\phi_2, \phi_3\}$ is $\{\ (\phi_1, T_1, T_8),\ (\phi_1, \phi_3, T_1),\ (\phi_2, T_1, T_8),\ (\phi_1, \phi_2, T_8),\ (\phi_2, \phi_3, T_1)\ \}$. From figure 2, it is clear that this collection of coordinate charts describes the toric variety that is obtained by the complete resolution of the orbifold obtained by turning on the blowup modes corresponding to the twist fields T_1 and T_8 (in that order) in the orbifold conformal field theory. As mentioned earlier, this is the most relevant tachyon sequence resulting in the least singular spacetime geometry.

Likewise we can analyze the other phases of the theory. Consider the convex hull $\{\phi_1, \phi_2\}$: this is also contained in the convex hulls $\{\phi_1, \phi_3\}$, $\{\phi_1, T_8\}$, $\{T_1, \phi_2\}$, $\{T_1, \phi_3\}$. Thus the collection of coordinate charts describing the toric variety in this phase is

$$\{\ (\phi_3, T_1, T_8),\ (\phi_2, T_1, T_8),\ (\phi_2, \phi_3, T_1),\ (\phi_1, \phi_3, T_8),\ (\phi_1, \phi_2, T_8)\ \}.$$

From figure 2, we see that this is the description of the complete resolution of the orbifold when the tachyon T_8 condenses first, followed by T_1: *i.e.*, we subdivide the toric fan in the sequence T_8, T_1, corresponding to the flip.

The convex hull $\{T_8, \phi_3\}$ is contained in the convex hulls $\{T_8, \phi_1\}$, $\{T_8, \phi_2\}$, giving the collection of coordinate charts as $\{ (\phi_1, \phi_2, T_1),\ (\phi_2, \phi_3, T_1),\ (\phi_1, \phi_3, T_1) \}$: this, from figure 2, corresponds to the partial blowup by T_1, *i.e.*, this is the endpoint of condensation of the tachyon T_1 alone.

Similarly, the convex hull $\{T_1, \phi_1\}$ is contained in the convex hulls $\{T_1, \phi_2\}$, $\{T_1, \phi_3\}$, giving the collection of coordinate charts $\{ (\phi_2, \phi_3, T_8),\ (\phi_1, \phi_3, T_8),\ (\phi_1, \phi_2, T_8) \}$: this, from figure 2, corresponds to the partial blowup by T_8, *i.e.*, this is the endpoint of condensation of the tachyon T_8 alone.

Finally the convex hull $\{T_1, T_8\}$ is not contained in any other convex hull: it gives the chart $\{ (\phi_1, \phi_2, \phi_3) \}$ that describes the unresolved orbifold singularity.

Flowlines

The two tachyons T_1 and T_8 have R-charges $R_1 = \frac{8}{13}$ and $R_1 = \frac{12}{13}$. Then the 1-loop running of the two FI parameters in this case (see (14)) is given by

$$r_1(\mu) = -5 \cdot \log \frac{\mu}{\Lambda} \ , \qquad\qquad r_2(\mu) = -1 \cdot \log \frac{\mu}{\Lambda} \ . \tag{38}$$

Now we can choose various bases for the $U(1) \times U(1)$ gauge fields by choosing appropriate linear combinations: these will therefore couple to the corresponding linear combinations of the FI parameters in the GLSM. The generic linear combination of the two FI parameters $\alpha_1 r_1 + \alpha_2 r_2$ has the 1-loop running

$$\alpha_1 r_1 + \alpha_2 r_2 = -(5\alpha_1 + \alpha_2) \cdot \log \frac{\mu}{\Lambda} \ . \tag{39}$$

From the coefficient, we see that this parameter is marginal if $5\alpha_1 + \alpha_2 = 0$: this describes a line in α-space, which is perpendicular to the ray $(5, 1)$ in r-space. Thus we can choose the basis for the $U(1) \times U(1)$ so that one linear combination couples to a (relevant) FI parameter that has nontrivial renormalization along the flow, while the other FI parameter is marginal along the flow. From (39), we see that this single relevant direction (perpendicular to the marginal one), lies along the ray $(5, 1)$: this is the flow-ray.

Using (39), we can get qualitative insight into the renormalization group trajectories that cross any of the phase boundaries: for instance, (39) gives

$$\frac{3r_1 - 2r_2}{13} \ = \ -1 \cdot \log \frac{\mu}{\Lambda} \ ,$$

$$\begin{aligned} \frac{8r_1 - r_2}{13} &= -3 \cdot \log \frac{\mu}{\Lambda} \ , \\ r_1 - (5+\epsilon) r_2 &= \epsilon \cdot \log \frac{\mu}{\Lambda} \ . \end{aligned} \tag{40}$$

These equations indicate that at low energies $\mu \ll \Lambda$, the 1-loop renormalization group flows drive the system towards the large r regions in r-space, *i.e.*, $r_1, r_2 \gg 0$, that are adjacent to the flow-ray $(5,1)$. There are two such regions: the convex hulls $\{T_8, \phi_3\}$ (for $\epsilon > 0$, *i.e.*, "below" the flow-ray $(5,1)$) and $\{\phi_2, \phi_3\}$ (for $\epsilon < 0$, *i.e.*, "above" the flow-ray $(5,1)$), for both of which $r_2 \ll \frac{3}{2} r_1 \ll 8 r_1$ holds. In the process of ending up in one of these regions, flowlines may cross one or more of the the (semi-infinite) phase boundaries passing through $(-13,0), (1,8), (2,3)$ and $(0,-13)$. We again remind the reader here that these straight flowlines are only valid away from the origin in r-space where all r_a are small: this is sufficient for our discussion here.

From the previous subsection, we see that these two phases arising as the endpoints of flowlines correspond to the decay modes of the unstable orbifold that represent the partial resolution by the condensation of the tachyon T_1 alone and the complete resolution by the condensation of the tachyon T_1 followed by T_8 in that sequence (which leads to the minimal singularity). It is interesting to interpret this result in terms of the toric description of tachyon condensation in this system [10] reviewed earlier. Recall that the most relevant tachyon is T_1 : after its condensation, the subsequent tachyon T_8 becomes marginal so that the blowup mode it corresponds to is now a modulus or flat direction, rather than a residual instability. This marginality of the residual (erstwhile tachyon) T_8 reflects the marginal $U(1)$ direction perpendicular to the tachyonic flow-ray $(5,1)$ in the GLSM. Thus the renormalization group in the GLSM drives the system along the flow-ray, maintaining a flat direction perpendicular to it. On the other hand, note that the tachyon T_1 remains tachyonic after condensation of T_8, so that the partial resolution by T_8 alone cannot result: the subsequent resolution by T_1 is *not* a flat direction but a residual instability.

This interpretation is further strengthened by the following: a flowline emanating in the orbifold phase (*i.e.*, the convex hull $\{T_1, T_8\}$) *below* the flow-ray $(5,1)$ necessarily crosses the (semi-infinite) phase boundary $(0,-13)$ to end up in the convex hull $\{T_8, \phi_3\}$. This trajectory corresponds to the most relevant tachyon T_1 turning on and condensing, resulting in a partial resolution. On the other hand, a flowline emanating *above* the flow-ray $(5,1)$ crosses the (semi-infinite) phase boundaries $(-13,0)$, $(1,8)$ and $(2,3)$ to end up in the convex hull $\{\phi_2, \phi_3\}$. This trajectory corresponds to the less relevant tachyon T_8 turning on first: this commences the partial resolution of the orbifold by the subdivision corresponding to T_8. As the flowline crosses the boundary $(1,8)$, the more relevant tachyon T_1 turns on which leads to the further resolution corresponding to the subsequent subdivision by T_1 : this is the phase represented by the convex hull $\{\phi_1, \phi_2\}$ corresponding to the flipped subdivision (T_8 followed by T_1). However

now the flowline crosses the boundary $(2,3)$ to end up finally in the phase $\{\phi_2, \phi_3\}$: note that this now represents the complete resolution by the tachyons but in the sequence T_1 followed by T_8. Thus in crossing the phase boundary $(2,3)$, there occurs a flip transition in which the sequence of partial resolutions of the orbifold by the two tachyons reverses, from T_8 followed by T_1 to T_1 and then T_8. Correspondingly the degree of singularity also changes to the less singular resolution.

We note here that the discussion above is just a detailed description in this example of the generalities of the previous section.

3.2 Including all three tachyons: the 3-parameter system

In this section, we study the decay of the $\mathbb{C}^3/\mathbb{Z}_{13}$ $(1,2,5)$ orbifold including all three tachyons present, *i.e.*, T_1, T_8, T_3 : these have R-charges $R_1 \equiv (\frac{1}{13}, \frac{2}{13}, \frac{5}{13}) = \frac{8}{13}$, $R_8 \equiv (\frac{8}{13}, \frac{3}{13}, \frac{1}{13}) = \frac{12}{13}$ and $R_3 \equiv (\frac{3}{13}, \frac{6}{13}, \frac{2}{13}) = \frac{11}{13}$. The GLSM in question has gauge group $U(1)^3$. The vacuum structure of the theory is governed by three independent FI parameters coupling to the three $U(1)$'s: these parameters run under the RG flow induced by the three tachyonic operators in the GLSM. The action of the $U(1)^3$ on the fields $\Psi_i \equiv \phi_1, \phi_2, \phi_3, T_1, T_8, T_3$ is given, as in (21), by $\Psi_i \to e^{iQ_i^a \lambda}\, \Psi_i$, where the charge matrix is

$$Q_i^a = \begin{pmatrix} 1 & 2 & 5 & -13 & 0 & 0 \\ 8 & 3 & 1 & 0 & -13 & 0 \\ 3 & 6 & 2 & 0 & 0 & -13 \end{pmatrix}. \tag{41}$$

(Again, we shall use this form due to the visibility of the tachyons, but in the more accurate form the first row would be replaced by (35) and the third row would be replaced by

$$\begin{pmatrix} 1 & 0 & 0 & 0 & -2 & 1 \end{pmatrix}, \tag{42}$$

which is $\frac{2}{13}$ times the second row plus $-\frac{1}{13}$ times the second.)

The D-term equations in this case are

$$\begin{aligned} D_1 &= |\phi_1|^2 + 2|\phi_2|^2 + 5|\phi_3|^2 - 13|T_1|^2 - r_1 = 0, \\ D_2 &= 8|\phi_1|^2 + 3|\phi_2|^2 + |\phi_3|^2 - 13|T_8|^2 - r_2 = 0, \\ D_3 &= 3|\phi_1|^2 + 6|\phi_2|^2 + 2|\phi_3|^2 - 13|T_3|^2 - r_3 = 0. \end{aligned} \tag{43}$$

Similarly we can obtain the counterparts of (37) of the 2-parameter analysis by studying the D-term equations obtained for various linear combinations of the three $U(1)$'s (the subscripts

denote the field(s) eliminated choosing two of the three D_is above, which are denoted by the superscripts)

$$\begin{aligned}
D_2^{12\prime} &= -|\phi_1|^2 + |\phi_3|^2 - 3|T_1|^2 + 2|T_8|^2 - \frac{3r_1 - 2r_2}{13} = 0 \ , \\
D_{2,3}^{23\,\prime} &= |\phi_1|^2 - 2|T_8|^2 - |T_3|^2 - \frac{2r_2 - r_3}{13} = 0 \ , \\
D_{2,1}^{13\,\prime} &= |\phi_3|^2 - 3|T_1|^2 + |T_3|^2 - \frac{3r_1 - r_3}{13} = 0 \ , \\
D_1^{12\prime} &= |\phi_2|^2 + 3|\phi_3|^2 - 8|T_1|^2 + |T_8|^2 - \frac{8r_1 - r_2}{13} = 0 \ , \\
D_1^{23\prime} &= -3|\phi_2|^2 - |\phi_3|^2 - 3|T_8|^2 + 8|T_3|^2 - \frac{3r_2 - 8r_3}{13} = 0 \ , \\
D_3^{12\prime} &= -3|\phi_1|^2 - |\phi_2|^2 - |T_1|^2 + 5|T_8|^2 - \frac{r_1 - 5r_2}{13} = 0 \ , \\
D_3^{13\prime} &= -|\phi_1|^2 - 2|\phi_2|^2 - 2|T_1|^2 + 5|T_3|^2 - \frac{2r_1 - 5r_3}{13} = 0 \ .
\end{aligned} \tag{44}$$

There are potentially $\binom{6}{4} = 15$ such D-term equations but some of them coincide due to the fact that some of the rays are coplanar, giving ten independent equations in (43), (44) above.

As before, the solutions to these D-term equations give collections of coordinate charts that characterize in general distinct toric varieties, depending on the FI parameters r_1, r_2, r_3: *i.e.*, varying r_1, r_2 and r_3 realizes several distinct phases of the theory (see figure 5). Analyzing the theory along the same lines as for the 2-parameter case, we find several distinct phase boundaries obtained as planes spanned by pairs of the phase bounding vectors $\phi_1 \equiv (1, 8, 3)$, $\phi_2 \equiv (2, 3, 6)$, $\phi_3 \equiv (5, 1, 2)$, $T_1 \equiv (-13, 0, 0)$, $T_8 \equiv (0, -13, 0)$, $T_3 \equiv (0, 0, -13)$: these can be read off as the six columns in the charge matrix (41). These planes defining phase boundaries intersect in pairs along rays emanating from the origin in r-space. The set of these intersection rays includes the six vectors ϕ_i, T_j above but also contains a new ray emanating from the origin out to the vector $\phi_0 \equiv (6, 9, 5)$, which arises as the intersection of the planes $\{\phi_1, \phi_3\}$ and $\{\phi_2, T_3\}$. The geometric relations amongst these vectors can be gleaned effectively by treating them as toric data. In particular, we see that certain subsets of these vectors are coplanar: specifically $\{\phi_1, \phi_2, T_8\}$ are coplanar, as are $\{\phi_2, \phi_3, T_1\}$, in other words, $\det(\phi_1, \phi_2, T_8) = 0$, and $\det(\phi_2, \phi_3, T_1) = 0$ (we can also see this by noting, *e.g.*, $2\phi_1 - \phi_2 + T_8 = 0$). By writing ϕ_2 and ϕ_1 as appropriate linear combinations of the other vectors, we find that ϕ_2 lies in the interior of the convex hulls $\{\phi_1, T_8, T_3\}$, $\{\phi_2, T_8, T_3\}$ (*e.g.*, we have $\phi_3 = 5\phi_1 + 3T_8 + T_3$) and $\phi_1 \in \{\phi_3, T_1, T_3\}$.

The various phases of the GLSM for this 3-parameter system can be obtained as in the 2-parameter case, by an analysis of the D-term equations, or equivalently by the operational method described in that subsection. Each phase in this case is a 3-dimensional convex hull, or

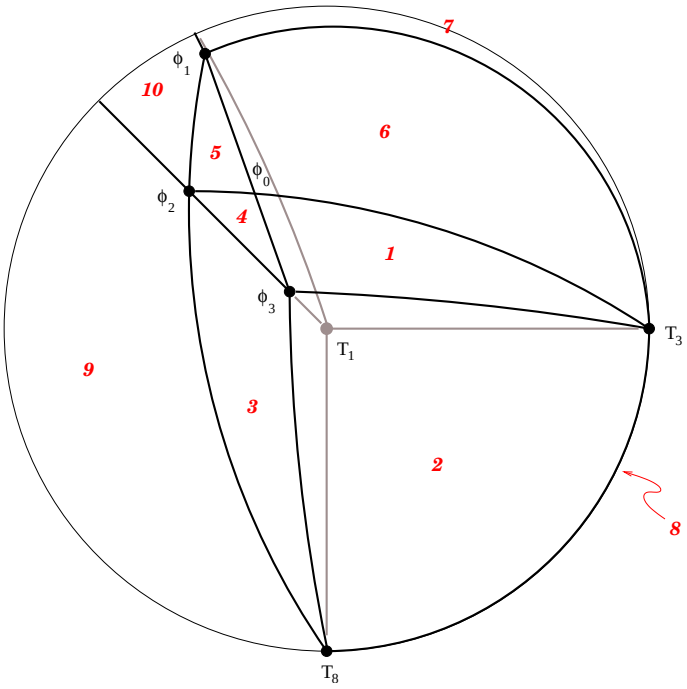

Figure 5: Phases of $\mathbb{C}^3/\mathbb{Z}_{13}$ $(1, 2, 5)$: the 3-parameter system of the three tachyons T_1, T_8, T_3. The seven intersection points ϕ_1, ϕ_2, ϕ_3, ϕ_0, T_1, T_8, T_3 of the phase boundary hyperplanes are shown as points on a unit sphere around the origin in r-space, along with the ten phases arising as convex hulls bounded by triples of the points.

3-simplex, defined by triples of the set of intersection rays $\{\phi_1, \phi_2, \phi_3, \phi_0, T_1, T_8, T_3\}$, bounded by the intersection planes mentioned above. Figure 5 shows the 3-dimensional phase diagram which has been drawn by plotting the projections of these seven rays on a unit sphere in r-space: in other words, we have shown the points $\frac{\phi_i}{\|\phi_i\|}$, $\frac{T_j}{\|T_j\|}$ as points on the unit sphere[14]. The view depicted in figure 5 is obtained by looking head-on "into" the sphere from the point antipodal to T_1, in other words, the line of sight is along the line $(1, 0, 0) \to (-1, 0, 0)$, in the direction of the ray T_1. The dark solid arcs are the intersections of the phase boundary hyperplanes with the unit sphere that lie on the hemisphere in direct view (*i.e.*, containing the point $\phi_3 \equiv (5, 1, 2)$) while the lighter arcs are the intersections that lie on the antipodally opposite hemisphere containing the point $T_1 \equiv (-13, 0, 0)$.

We now outline the operational method described in the 2-parameter discussion to obtain

[14]For the benefit of the reader, we mention here that this is probably the most convenient method to accurately obtain a visualization of the relations between the rays and thence the various phases: figure 5 was obtained by first plotting these points on an actual racquetball(!) after finding that the stereographic projection onto a 2-plane intersecting the unit sphere yielded results that were difficult to interpret.

the ten phases in Figure 5. Consider, for instance, the phase $r_1, r_2, r_3 \ll 0$, *i.e.*, the convex hull $\{T_1, T_8, T_3\}$: these fields alone acquire nonzero expectation values and the remaining massless fields describe the coordinate chart (ϕ_1, ϕ_2, ϕ_3), *i.e.*, the unresolved orbifold singularity. Likewise, in the convex hull $\{\phi_1, \phi_2, T_1\}$, the residual massless fields describe the chart (ϕ_3, T_8, T_3). The procedure is clear: each convex hull $\{\psi_1, \psi_2, \psi_3\}$ yields a description of a coordinate chart given by the complement of these fields in the collection of the six vectors $\{\phi_i, T_j\},\ i = 1, 2, 3,\ j = 1, 8, 3$. In addition to this of course, we note as before that a given convex hull may be itself contained in other convex hulls: thus each convex hull yields a collection of coordinate charts which then describes a toric variety. Furthermore, the convex hulls thus obtained using triples of these six vectors in general intersect giving possibly new vectors: as we have seen above, the only new vector in this case is ϕ_0. By carefully studying the 3-dimensional phase diagram in Figure 5, we can see that the ten distinct phases[15] are as given in Table 1 and Table 2: the first column labels the phase number as shown in figure 5, the second column gives the phases as intersections of convex hulls, the third gives the collection of coordinate charts valid in each phase while the fourth column then gives the interpretation of each phase in accord with Figure 2.

Table 1: Stable phases of $\mathbb{C}^3/\mathbb{Z}_{13}$ $(1, 2, 5)$

1	$\{\phi_3, \phi_0, T_3\} = \{\phi_1, T_3, \phi_3\} \cap \{\phi_2, T_3, \phi_3\} \cap \{\phi_3, T_1, T_3\} \cap \{\phi_1, T_8, T_3\} \cap \{\phi_2, T_8, T_3\}$	(ϕ_2, T_1, T_8), (ϕ_1, T_1, T_8), (ϕ_1, ϕ_2, T_8), (ϕ_2, ϕ_3, T_1), (ϕ_1, ϕ_3, T_1)	Partial resolution by T_1 followed by T_8 (minimal singularity)
2	$\{\phi_3, T_3, T_8\} = \{\phi_3, T_3, T_8\} \cap \{\phi_1, T_3, T_8\} \cap \{\phi_2, T_3, T_8\}$	(ϕ_1, ϕ_2, T_1), (ϕ_2, ϕ_3, T_1), (ϕ_1, ϕ_3, T_1)	Partial resolution by T_1
3	$\{\phi_3, \phi_2, T_8\} = \{\phi_2, \phi_3, T_8\} \cap \{\phi_1, \phi_3, T_8\} \cap \{\phi_3, T_1, T_8\} \cap \{\phi_1, T_8, T_3\} \cap \{\phi_2, T_8, T_3\}$	(ϕ_1, T_1, T_3), (ϕ_2, T_1, T_3), (ϕ_1, ϕ_2, T_3), (ϕ_2, ϕ_3, T_1), (ϕ_1, ϕ_3, T_1)	Partial resolution by T_1 and T_3
4	$\{\phi_3, \phi_2, \phi_0\} = \{\phi_1, T_8, \phi_3\} \cap \{\phi_2, T_3, \phi_3\} \cap \{\phi_1, T_8, T_3\} \cap \{\phi_2, \phi_3, T_3\} \cap \{\phi_3, T_1, T_3\} \cap \{\phi_2, T_3, T_8\} \cap \{\phi_1, \phi_2, \phi_3\}$	(ϕ_2, T_1, T_3), (ϕ_1, T_1, T_8), (ϕ_2, ϕ_3, T_1), (ϕ_1, T_1, T_8), (ϕ_1, ϕ_2, T_8), (ϕ_1, ϕ_3, T_1), (T_1, T_8, T_3)	Complete resolution by T_1 followed by T_8, T_3 (minimal singularity)

[15]Note that Figure 5 can be thought of as a picture of a triangulation of the unit sphere where each triangle is an intersection of the corresponding convex hull with the unit sphere. Then we know the Euler characteristic for the sphere to be $\chi = 2 = Faces + Vertices - Edges$, which gives the $10 + 7 - 2 = 15$ edges or phase boundaries shown in Figure 5.

Table 2: Unstable phases of $\mathbb{C}^3/\mathbb{Z}_{13}$ $(1,2,5)$

5	$\{\phi_0,\phi_2,\phi_1\} = \{\phi_1,\phi_2,\phi_3\} \cap \{\phi_1,\phi_2,T_3\} \cap \{\phi_1,\phi_3,T_1\} \cap \{\phi_1,T_8,\phi_3\} \cap \{\phi_2,T_3,T_1\} \cap \{\phi_3,T_3,T_1\} \cap \{\phi_1,T_1,T_8\}$	(T_1,T_8,T_3), (ϕ_3,T_1,T_8), (ϕ_2,T_3,T_8), (ϕ_2,T_1,T_3), (ϕ_1,ϕ_3,T_8), (ϕ_1,ϕ_2,T_8), (ϕ_2,ϕ_3,T_1)	Complete resolution by T_8 followed by T_1, T_3 (flip)
6	$\{\phi_0,\phi_1,T_3\} = \{\phi_1,\phi_2,T_3\} \cap \{\phi_1,\phi_3,T_3\} \cap \{\phi_3,T_1,T_3\} \cap \{\phi_2,T_1,T_3\} \cap \{\phi_1,T_8,T_3\}$	(ϕ_3,T_1,T_8), (ϕ_2,T_1,T_8), (ϕ_1,ϕ_2,T_8), (ϕ_1,ϕ_3,T_8), (ϕ_2,ϕ_3,T_1)	Partial resolution by T_8 followed by T_1 (flip)
7	$\{\phi_1,T_1,T_3\} = \{\phi_1,T_1,T_3\} \cap \{\phi_2,T_1,T_3\} \cap \{\phi_3,T_1,T_3\}$	(ϕ_2,ϕ_3,T_8), (ϕ_1,ϕ_3,T_8), (ϕ_1,ϕ_2,T_8)	Partial resolution by T_8
8	$\{T_1,T_8,T_3\}$	(ϕ_1,ϕ_2,ϕ_3)	Unresolved orbifold
9	$\{\phi_2,T_1,T_8\} = \{\phi_2,T_1,T_8\} \cap \{\phi_3,T_1,T_8\} \cap \{\phi_1,T_1,T_8\}$	(ϕ_1,ϕ_3,T_3), (ϕ_1,ϕ_2,T_3), (ϕ_2,ϕ_3,T_3)	Partial resolution by T_3
10	$\{\phi_1,\phi_2,T_1\} = \{\phi_1,\phi_2,T_1\} \cap \{\phi_1,T_1,T_8\} \cap \{\phi_3,\phi_1,T_1\} \cap \{\phi_2,T_1,T_3\} \cap \{\phi_3,T_1,T_3\}$	(ϕ_3,T_3,T_8), (ϕ_2,ϕ_3,T_3), (ϕ_2,T_8,T_3), (ϕ_1,ϕ_3,T_8), (ϕ_1,ϕ_2,T_8)	Partial resolution by T_8 and T_3

The 1-loop running of the FI parameters

$$r_a(\mu) = \Big(\sum_i Q_i^a\Big) \cdot \log\frac{\mu}{\Lambda}\ , \qquad\qquad a = 1,2,3, \tag{45}$$

is given in this case by

$$\begin{aligned} r_1(\mu) &= -5 \cdot \log\frac{\mu}{\Lambda}\ , \\ r_2(\mu) &= -1 \cdot \log\frac{\mu}{\Lambda}\ , \\ r_3(\mu) &= -2 \cdot \log\frac{\mu}{\Lambda}\ , \end{aligned} \tag{46}$$

Thus the generic linear combination of the three $U(1)$'s couples to a FI parameter

$$\alpha_1 r_1 + \alpha_2 r_2 + \alpha_3 r_3 = -(5\alpha_1 + \alpha_2 + 2\alpha_3) \cdot \log\frac{\mu}{\Lambda}\ , \tag{47}$$

which is marginal if $5\alpha_1 + \alpha_2 + 2\alpha_3 = 0$: this now describes a plane perpendicular to the ray emanating from the origin out to $(5,1,2)$ in r-space. Thus we can choose a basis for the charges of the fields under the three $U(1)$'s so that one linear combination is relevant, coupling to a FI parameter that has nontrivial renormalization along the flow, while the other two FI parameters are marginal along the flow. This single relevant direction defining the directionality

of all flowlines lies along the ray emanating from the origin $(0,0,0)$ passing through $(5,1,2)$, in other words, ϕ_3 can be identified as the flow-ray in 3-dimensional r-space. By studying various linear combinations (47), we see that the 1-loop renormalization group flows drive the system to the large r regions in r-space, *i.e.*, $r_1, r_2, r_3 \gg 0$, that are adjacent to the flow-ray $\phi_3 \equiv (5,1,2)$. From Figure 5, we see that there are four such phases, labelled by $\mathbf{1}, \mathbf{2}, \mathbf{3}, \mathbf{4}$: these are the convex hulls $\{\phi_3, \phi_0, T_3\}, \{\phi_3, T_3, T_8\}, \{\phi_3, T_8, \phi_2\}, \{\phi_3, \phi_2, \phi_0\}$, respectively. These four stable phases are listed in Table 1.

The other six of the ten represent unstable phases, listed in Table 2: renormalization group flowlines emanate from these phases and end on the stable ones. Thus for initial conditions for the geometry as any of these phases, small fluctuations will force the geometry to dynamically evolve to one of the four stable phases.

3.3 The space of geometries and the RG trajectories

As in the 2-parameter case, it is interesting to revisit the toric description of tachyon condensation to shed light on the stability of the four phases and instability of the other six. Recall that T_1 was the most relevant tachyon: thus the dominant decay channel for the unstable orbifold involves the condensation of T_1 first, in other words, the partial resolution of the orbifold by T_1. After condensation of T_1, subsequent tachyons T_8 and T_3 become marginal so that the blowup modes they correspond to are moduli, not residual instabilities. Thus subsequent resolutions by T_8 or T_3 represent flat directions of the full tachyon potential: the existence of these two independent flat directions in spacetime is reflected by the existence of the plane of the two marginal $U(1)$'s in the GLSM[16]. Thus the renormalization group drives the system to the large r region along the direction of the flow-ray, preserving a plane of flat directions. The possibility of turning on the residual moduli yields four possible distinct stable endpoints, listed in Table 1. It is also of course possible for the tachyons to condense in other sequences. In this case however, recall that the tachyon T_1 remains tachyonic after condensation of either T_8 or T_3: in other words, the tachyon T_1, if subsequent, is always a residual instability, not a flat direction. This is reflected in the fact that all of the stable phases involve (partial) resolutions by the tachyon T_1, in other words, the (most relevant) tachyon T_1 always does condense eventually.

Further light is shed on the possible trajectories in the space of geometries by studying the projections of these phases onto the plane of marginal $U(1)$'s. A basis for the two marginal $U(1)$'s is given by the charge matrix[17] with entries in the two rows given by $\frac{1}{13}(Q_i^1 - 5Q_i^2,\ Q_i^3 - 2Q_i^2)$

[16] In general, it is possible that the flat directions in spacetime are appropriate combinations of the subsequent tachyonic twisted states in the GLSM.

[17] Equivalently we could use the charge matrix corresponding to (27).

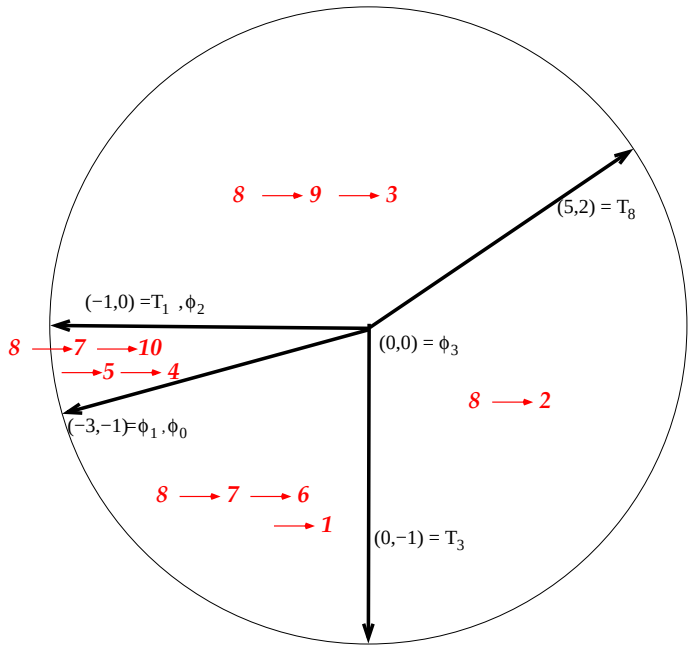

Figure 6: The marginal hyperplane and RG trajectories in $\mathbb{C}^3/\mathbb{Z}_{13}$ $(1,2,5)$: shown here is the marginal hyperplane normal to the flow-ray ϕ_3 (taken as the origin). The dark arrows mark the intersections of the marginal hyperplane with the phase boundaries. Identifying the convex hulls that overlap with each of the regions (see figure 5) gives the four trajectories shown.

with Q_i^a given in (41) :

$$Q_i^a = \begin{pmatrix} -3 & -1 & 0 & -1 & 5 & 0 \\ -1 & 0 & 0 & 0 & 2 & -1 \end{pmatrix}. \tag{48}$$

Note that by construction, $\sum_i Q_i^a = 0,\ i = 1,2$, indicating marginality. Now treating this as an effective 2-parameter system, we can plot the phases in the vicinity of the flow-ray $\phi_3 \equiv (5,1,2)$, defined as the origin, by drawing rays emerging from the origin out to each of the other points (see figure 6). Clearly there are four regions. Identifying the subsets of the ten phases from Table 1 and Table 2 that overlap with each of these four regions gives the following four trajectories (see Figure 6):

1. Unresolved orbifold [8] → partial resolution by T_8 [7] → partial resolution by T_8 and T_1 (in that sequence) [6] → partial resolution by T_1 and T_8 (minimal singularity) [1].

2. Unresolved orbifold [8] → partial resolution by T_1 [2].

3. Unresolved orbifold [8] → partial resolution by T_3 [9] → partial resolution by T_3 and T_1 [3].

4. Unresolved orbifold [8] $\rightarrow$ partial resolution by T_8 [7] $\rightarrow$ partial resolution by T_8 and T_3 [10] $\rightarrow$ partial resolution by T_8, T_3 and T_1 (in that sequence) [5] $\rightarrow$ partial resolution by T_1, T_3 and T_8 (minimal singularity) [4].

For the 3-parameter system, we have seen that there are ten phases or regions in r-space. From the point of view of the renormalization group for the GLSM, each phase is a fixed point, stable or unstable. All of the above RG flowlines emanate from the unresolved orbifold phase **8**, which is the UV fixed point. The infrared fixed point in the trajectory k above is the stable phase **k** in Table 1. The trajectories 1 and 4 involve flip transitions: these occur in the region given by the convex hull $\{\phi_1, \phi_3, T_8, T_1\}$ in figure 2. They involve a reversal of the sequence of condensation of tachyons from T_8, T_1 to T_1, T_8 and therefore of the blowups corresponding to them. This involves a blowdown of a divisor and a blowup of a topologically distinct divisor resulting in a singularity of smaller degree.

Thus the RG trajectories **2** and **3** flow directly from an unstable UV phase to a stable IR phase. However the trajectories **1** and **4** that involve flip transitions may pass arbitrarily close to a unstable IR fixed point (*i.e.*, an unstable phase) before eventually flowing to a stable IR fixed point[18]. In this sense, one could think of the blowdown+blowup as the combination of an irrelevant and a relevant operator in the GLSM. Indeed this is borne out by the coefficient of the FI parameter r^{eff} for the corresponding relative $U(1)$ in Sec. 2.2.

The above $\mathbb{Z}_{13}$ example was in the context of the Type 0 string theory, where as we have seen, the (nonsupersymmetric) terminal singularity $\mathbb{C}^3/\mathbb{Z}_2\ (1,1,1)$ does appear in the spectrum of stable phases under tachyon condensation. Similar analyses can be performed in the context of the Type II string. A key observation here is that for every stable phase in the Type II theory, the residual singularities are all supersymmetric. Furthermore, in a stable phase, some of the sizes of curves and surfaces on the threefold (measured by the r_a's) may lie in the marginal hyperplane and thus remain finite in the infrared. Thus, although the region near the original nonsupersymmetric singular point generally inflates to infinite size, residual supersymmetric singularities may remain at finite distance from each other in the infrared. Those finite distances correspond to parameters in the infrared theory – parameters which are clearly determined by the corresponding marginal operators at high energy.[19]

[18]This is reminiscent of the supersymmetric flows that flow from $\mathbb{C}^3/\mathbb{Z}_N$ geometries towards $\mathbb{C}^2/\mathbb{Z}_N$ before flowing finally to flat space [21]. Along these lines, it would perhaps be interesting to ask what a D-brane probe sees during a flip transition.

[19]Note, however, that not all high energy marginal operators have such a geometric interpretation, and it is not clear that the non-geometric ones survive to the infrared theory. We thank Emil Martinec and Greg Moore for discussions on this point.

4 Tachyon decay products in two dimensions

To avoid giving the impression that the phenomenon of stable and unstable phases, with the stable ones related by marginal operators in the infrared, in purely a three-dimensional phenomenon, we briefly give an example in two dimensions which exhibits the same phenomenon.

4.1 An example

We begin with a charge matrix

$$Q_i^a = \begin{pmatrix} 1 & -1 & 6 & -6 & 0 \\ 0 & 0 & -1 & 2 & -1 \\ 0 & -1 & 3 & -1 & 0 \end{pmatrix}. \tag{49}$$

To clarify the geometry, we can use some (non-invertible) row operations to find

$$\begin{pmatrix} 1 & 0 & -6 \\ 3 & 0 & -6 \\ 5 & 12 & -6 \end{pmatrix} \begin{pmatrix} 1 & -1 & 6 & -6 & 0 \\ 0 & 0 & -1 & 2 & -1 \\ 0 & -1 & 3 & -1 & 0 \end{pmatrix} = \begin{pmatrix} 1 & 5 & -12 & 0 & 0 \\ 3 & 3 & 0 & -12 & 0 \\ 5 & 1 & 0 & 0 & -12 \end{pmatrix} \tag{50}$$

This is in fact the orbifold $\mathbb{C}^2/\mathbb{Z}_{12}$ $(1,5)$, which has three tachyons (visible in the second form of the charge matrix).

The classical vacua of the theory are found by studying the D-terms (corresponding to the first form of the charge matrix):

$$\begin{aligned} D_1 &= |\phi_1|^2 - |\phi_2|^2 + 6|T_1|^2 - 6|T_2|^2 - r_1 = 0, \\ D_2 &= -|T_1|^2 + 2|T_2|^2 - |T_3|^2 - r_2 = 0, \\ D_3 &= -|\phi_2|^2 + 3|T_1|^2 - |T_2|^2 - r_3 = 0. \end{aligned} \tag{51}$$

As in the previous example, the vectors bounding the phases are $\phi_1 \equiv (1,0,0)$, $\phi_2 \equiv (-1,0,-1)$, $T_1 \equiv (6,-1,3)$, $T_2 \equiv (-1,2,-1)$, and $T_3 \equiv (0,-1,0)$ together with $\phi_0 \equiv (3,-1,0)$ which arises as the intersection of the planes $\{\phi_1, T_3\}$ and $\{\phi_2, T_1\}$.

There are eight phases in this example: six unstable and two stable phases. One stable phase corresponds to a complete resolution of the singularity, which consists of a chain of three rational curves, with the outer curves having self-intersection -3 and the middle curve having self-intersection -2. This follows from the Hirzebruch-Jung continued fraction expansion

$$\frac{12}{5} = 3 - \frac{1}{2 - \frac{1}{3}}$$

whose coefficients give the self-intersections. In the other stable phase, the middle curve is not resolved, but rather appears as a $\mathbb{C}^2/\mathbb{Z}_2$ singularity. The size of the middle curve serves as the marginal parameter in the infrared. (The two outer curves blow up to infinite size, but the middle curve remains finite size, even in the "smooth" stable phase.) In the other stable phase, the marginal parameter is a twist field for the orbifold.

We summarize the data for this example in Table 3 similar to those of the previous section. There are six possible types of trajectories, passing through the various phases:

$$\begin{aligned} 1 \to 2 \to 7 \\ 1 \to 4 \to 7 \\ 1 \to 4 \to 6 \to 8 \\ 1 \to 3 \to 6 \to 8 \\ 1 \to 3 \to 5 \to 8 \\ 1 \to 2 \to 5 \to 8 \end{aligned} \tag{52}$$

Table 3: Phases of $\mathbb{C}^2/\mathbb{Z}_{12}$ $(1,5)$

1	$\{T_1, T_2, T_3\}$	(ϕ_1, ϕ_2)	Orbifold
2	$\{\phi_2, T_2, T_3\} = \{\phi_2, T_2, T_3\} \cap \{\phi_1, T_2, T_3\}$	(ϕ_1, T_1), (ϕ_2, T_1)	Partial resolution by T_1
3	$\{\phi_0, T_1, T_3\} = \{\phi_1, T_1, T_3\} \cap \{\phi_2, T_1, T_3\}$	(ϕ_1, T_2), (ϕ_2, T_2)	Partial resolution by T_2
4	$\{\phi_1, T_1, T_2\} = \{\phi_1, T_1, T_2\} \cap \{\phi_2, T_1, T_2\}$	(ϕ_1, T_3), (ϕ_2, T_3)	Partial resolution by T_3
5	$\{\phi_0, \phi_2, T_3\} = \{\phi_1, \phi_2, T_3\} \cap \{\phi_1, T_2, T_3\} \cap \{\phi_2, T_1, T_3\}$	(ϕ_1, T_1), (T_1, T_2), (ϕ_2, T_2)	Partial resolution by T_1 and T_2
6	$\{\phi_0, \phi_1, T_1\} = \{\phi_1, \phi_2, T_1\} \cap \{\phi_2, T_1, T_2\} \cap \{\phi_1, T_1, T_3\}$	(ϕ_1, T_3), (T_2, T_3), (ϕ_2, T_2)	Partial resolution by T_2 and T_3
7	$\{\phi_1, \phi_2, T_2\} = \{\phi_1, \phi_2, T_2\} \cap \{\phi_1, T_2, T_3\} \cap \{\phi_2, T_1, T_2\}$	(ϕ_1, T_3), (T_1, T_3), (ϕ_2, T_1)	Partial resolution by T_1 and T_3
8	$\{\phi_0, \phi_1, \phi_2\} = \{\phi_1, T_2, T_3\} \cap \{\phi_2, T_1, T_2\} \cap \{\phi_1, \phi_2, T_1\} \cap \{\phi_1, \phi_2, T_3\}$	(ϕ_1, T_3), (T_2, T_3), (T_1, T_2), (ϕ_2, T_1)	Complete resolution

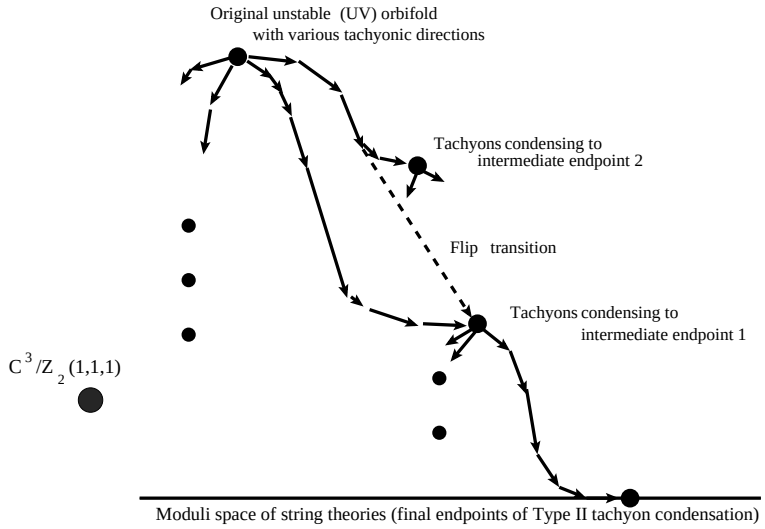

Figure 7: A heuristic picture of an unstable (UV) orbifold with several relevant directions: two distinct tachyons in $\mathbb{C}^3/\mathbb{Z}_N$ condense to distinct endpoints, with a possible flip transition between them. Intermediate endpoint I stemming from condensation of a more relevant tachyon is less singular than intermediate endpoint II. The *final* endpoint of condensation of all tachyons for Type II string theories is the smooth moduli space. Type 0 theories however admit a truly terminal singularity $\mathbb{C}^3/\mathbb{Z}_2$ $(1,1,1)$ in the spectrum of decay endpoints.

5 Conclusions and discussion

We have seen that the geometric (Higgs branch) phases of a GLSM for a nonsupersymmetric orbifold correspond to the possible spacetime geometries that can result as the endpoint of tachyon condensation. The stability of these phases is related to the possible existence of flip transition trajectories that flow towards the more stable phases which correspond to the condensation of the most relevant tachyon sequence. In addition to the Higgs branch vacua, the GLSM also exhibits nonclassical Coulomb branch vacua: it would be interesting to interpret these from the point of view of the nonlinear sigma model describing string propagation on the target space geometry.

We have described flip transitions in this paper from the point of view of the GLSM and its interrelations with the toric description in [10]. While at the level of the GLSM, flips appear structurally similar to flop transitions in supersymmetric Calabi-Yaus, the physics they describe is quite different, as we have seen. It would be interesting to understand the role of nonperturbative (in the string coupling) effects such as D-branes in these theories, in part with a view to understanding similarities and differences in the physics of (nonsupersymmetric)

flips and (supersymmetric) flops. This is perhaps closely tied to a better understanding of the geometry in the vicinity of the nonsupersymmetric analogue of the conifold singularity itself, as well as its deformations. It would also be interesting to obtain a better understanding of the connection between worldsheet RG flow and direct time evolution in spacetime, and the time evolution of flip transition trajectories.

The GLSM analysis here gives some insight into the space of geometries and the off-shell closed string tachyon potential. Intuitively we expect that the distinct phases of GLSMs correspond to the various extrema of the tachyon potential. Then thinking of an unstable $\mathbb{C}^3/\mathbb{Z}_N$ orbifold as the UV fixed point with several unstable directions (see figure 7), we know from [10] that the *final* endpoints of tachyon condensation do not include terminal singularities and are always supersymmetric spaces (generally smooth spaces such as supersymmetric Calabi-Yau manifolds, with supersymmetric singularities also permitted) for Type II string theories. These final endpoints can be thought of as the culmination of condensation of all tachyons, chiral and nonchiral[20], and are the absolute minima of the tachyon potential. Thus the depth of the tachyon potential for a given orbifold is basically the height of the orbifold "hill" maximum above the absolute minima, *i.e.*, the (smooth) moduli space.

In an off-shell formulation of string theory, one expects that the tachyon potential[21] for a given orbifold $\mathbb{C}^3/\mathbb{Z}_N$ $(1,p,q)$ is a function $V(T)$ describing the dynamics of all the tachyon fields T_i in the system, with parameters N,p,q. This is to be treated with some care since a given $\mathbb{Z}_N$ $(1,p,q)$ orbifold can be relabelled in terms of various distinct parameters p,q, so that naive expressions for $V(T)$ might in fact be incorrect. [22] gives a conjecture for the depth of the potential $V(T)$ for $\mathbb{C}/\mathbb{Z}_N$. However unlike $\mathbb{C}/\mathbb{Z}_N$, where the most relevant tachyon decay channel leads to flat space, $\mathbb{C}^2/\mathbb{Z}_N$ and $\mathbb{C}^3/\mathbb{Z}_N$ orbifolds typically do not decay to supersymmetric spaces via the most relevant tachyon: the endpoints themselves are typically unstable to tachyon condensation via subsequent tachyons. Expressions involving condensation of a single tachyon appear in [23, 25, 20]. Using these, one can thus attempt an iterative guess for the depth $V(T)$ by summing over all tachyons (mass M^2, R-charge R) present in the

[20] As seen in [10] (in the Type II example discussed there), condensation of purely chiral tachyons will in general result in geometric terminal singularities which will then continue to decay via the nonchiral tachyonic blowup modes to finally result in supersymmetric spaces.

[21] Note that the status of the tachyon potential for noncompact codimension three and two singularities is somewhat different from that for $\mathbb{C}/\mathbb{Z}_N$: under tachyon condensation, while the asymptotic geometry remains an S^1 for the latter, the asymptotics changes for $\mathbb{C}^3/\mathbb{Z}_N$ and $\mathbb{C}^2/\mathbb{Z}_N$, making it hard to compare, say, energies of the geometries at early and late times. The heuristic picture of the tachyon potential in figure 7 is thus best interpreted as a formal picture of the "space of string theories", without a precise quantitative physical measure thereof, at least for the present.

orbifold,

$$V(T) \sim \sum_k M_{T_k}^2 \sim \sum_k (R_k - 1) \ . \tag{53}$$

It is important to realize that subsequent tachyons can potentially become irrelevant in $\mathbb{C}^3/\mathbb{Z}_N$ [10], so that care must be used in evaluating the sum in this expression. It is then reasonable to expect that this sum in fact converges to a quantity that involves only the parameters N, p, q for the original unstable orbifold that we began with (note that this final expression must be independent of possible redefinitions of the k_i labelling the same physical orbifold): it is further tempting to ask if there are connections to the g_{cl} conjecture of [9]. It would be interesting to pursue these lines of thought further to get deeper insights into the tachyon potential and the "space of string theories".

Acknowledgments: It is a pleasure to thank Allan Adams, Paul Aspinwall, Atish Dabholkar, Emil Martinec, Ilarion Melnikov, Shiraz Minwalla, Greg Moore, Sunil Mukhi and Ronen Plesser for useful discussions. This work is partially supported by NSF grant DMS-0301476.

References

[1] See, *e.g.*, A. Sen, "Tachyon dynamics in open string theory", [hep-th/0410103], and references therein.

[2] E. Martinec, "Defects, decay and dissipated states", [hep-th/0210231].

[3] M. Headrick, S. Minwalla, T. Takayanagi, "Closed string tachyon condensation: an overview", [hep-th/0405064].

[4] W. Taylor, B. Zwiebach, "D-branes, tachyons and string field theory", [hep-th/0311017].

[5] E. Witten, in *Quantum fields and strings: a course for mathematicians*, see, *e.g.*, Lecture 12 at http://www.cgtp.duke.edu/QFT/spring/.

[6] K. Hori, Trieste Lectures on Mirror Symmetry, Proceedings, ICTP Spring School on superstrings and related matters, Mar 2002 (available on Spires).

[7] A. Adams, J. Polchinski, E. Silverstein, "Don't panic! Closed string tachyons in ALE space-times", [hep-th/0108075].

[8] C. Vafa, "Mirror symmetry and closed string tachyon condensation", [hep-th/0111051].

[9] J. Harvey, D. Kutasov, E. Martinec, G. Moore, "Localized tachyons and RG flows" [hep-th/0111154] ;

[10] David R. Morrison, K. Narayan, M. Ronen Plesser, "Localized tachyons in $\mathbb{C}^3/\mathbb{Z}_N$", [hep-th/0406039].

[11] E. Witten, "Phases of $\mathcal{N}$=2 theories in two dimensions", [hep-th/9301042].

[12] D. R. Morrison, M. R. Plesser, "Summing the instantons: quantum cohomology and mirror symmetry in toric varieties", [hep-th/9412236].

[13] J. David, M. Gutperle, M. Headrick, S. Minwalla, "Closed string tachyon condensation on twisted circles", [hep-th/0111212].

[14] T. Sarkar, "Brane probes, toric geometry and closed string tachyons", [hep-th/0206109].

[15] E. Martinec, G. Moore, "On decay of K-theory", [hep-th/0212059].

[16] S. Minwalla, T. Takayanagi, "Evolution of D-branes under closed string tachyon condensation", [hep-th/0307248].

[17] S.-J. Sin, "Comments on the fate of unstable orbifolds", [hep-th/0308028].

[18] S. Lee and S.-J. Sin, "Localized tachyon condensation and G-parity conservation", [hep-th/0312175].

[19] G. Moore and A. Parnachev, "Localized tachyons and the quantum McKay correspondence", [hep-th/0403016].

[20] T. Sarkar, "On localized tachyon condensation in $\mathbb{C}^2/\mathbb{Z}_N$ and $\mathbb{C}^3/\mathbb{Z}_N$", [hep-th/0407070].

[21] K. Narayan, M. Ronen Plesser, "Coarse-graining quivers", [hep-th/0309171].
See also K. Narayan, "Blocking up D-branes: matrix renormalization ?", [hep-th/0211110].

[22] A. Dabholkar, "Tachyon condensation and black hole entropy", [hep-th/0111004].

[23] A. Dabholkar, C. Vafa, "tt^* geometry and closed string tachyon potential", [hep-th/0111155].

[24] A. Dabholkar, A. Iqubal, J. Raeymaekers, "Off-shell interactions for closed string tachyons", [hep-th/0403238].

[25] S.-J. Sin, "Localized tachyon mass and a g-theorem analogue", [hep-th/0308015].